Stimulation of Gαq Promotes Stress Granule Formation

Androniqi Qifti, Lela Jackson, Ashima Singla, Osama Garwain and Suzanne Scarlata

Department of Chemistry and Biochemistry, Worcester Polytechnic Institute, Worcester, MA 01609

ABSTRACT

During adverse environmental conditions, mammalian cells regulate protein production by sequestering the translation machinery in membraneless organelles (i.e. stress granules) whose formation is carefully regulated. In this study, we show a direct connection between G protein signaling and stress granule formation through phospholipase Cβ (PLCβ). In cells, PLCβ localizes to both the cytoplasm and plasma membrane. We find that a major population of cytosolic PLCβ binds to stress granule proteins; specifically, eIF5A and Ago2, whose RNA-induced silencing activity is halted under stress. PLCβ1 is activated by Gαq in response to hormones and neurotransmitters and we find that activation of Gαq shifts the cytosolic population of PLCβ1 to the plasma membrane, releasing stress granule proteins. This release is accompanied by the formation of intracellular particles containing stress granule markers, an increase in the size and number of particles, and a shift of cytosolic RNAs to larger sizes consistent with cessation of transcription. Arrest of protein synthesis is seen when the cytosolic level of PLCβ1 is lowered by siRNA or by osmotic stress, but not cold, heat or oxidative stress causes similar behavior. Our results fit a simple thermodynamic model in which eIF5a and its associated proteins partition into particles after release from PLCβ1 due to Gαq stimulation. Taken together, our studies show a link between Gαq-coupled signals and transcription through stress granule formation.

INTRODUCTION

When cells are subjected to environmental stress, they halt the production of many housekeeping proteins to preserve resources for the synthesis of proteins that will help the cell alleviate the particular stress. These stalled transcription complexes, called stress granules, are thought to act as junctures that protect non-translated mRNAs from degradation until the stress is removed while allowing the synthesis of other proteins (for review see (*1, 2*)). Stress granules are distinct from processing bodies or P-bodies that store and process mRNA, although they have also been observed under non-stress conditions and can act as waiting stations that allow cells to decide whether mRNAs need to be degraded, stored or enter the translational machinery. Physically,

stress granules are membraneless aggregates composed of non-translating mRNAs, translation initiation complexes, poly (A)-binding protein, and many additional mRNA related proteins (*3*). They consist of a packed core with loosely associated peripheral proteins (*4*). Stress granules appear when cells undergo stress such as cold or heat shock, exposure to toxic molecules, oxidative stress, hypo- or hyper-osmolarity, UV irradiation and nutrient deprivation. The molecular mechanisms that transmit these different stresses into the cell interior are unclear.

Stress granules have been implicated in the pathogenesis of various diseases such as cancer, neurodegeneration and viral infections (*1, 5*). Many stress granule proteins contain disordered domains and these regions play important roles in the liquid-like nature of stress granules. Neuronal cells, in particular, contain many proteins with disordered domains and so it is not surprising that some neurological diseases (e.g. ALS) have been attributed to abnormal stability of stress granules (see (*6*)). Thus, it is important that cells have mechanisms to prevent premature formation of stress granules, and to insure their reversible assembly and disassembly.

While stress granules primarily contain proteins associated with translation, it is notable that argonaute 2 (Ago2) can be found in these domains (see (*7*)). Ago2 is the main nuclease component of the RNA-induced silencing complex (*8*). Ago2 binds small, silencing RNAs in their double-stranded form, and holds the guide strand after the passenger strand is degraded to allow hybridization with a target mRNA. If pairing between the passenger strand and the mRNA is perfect, as is the case in exogenous siRNAs, then Ago2 will undergo conformational changes that result in RNA degradation. Alternately, if pairing is imperfect, as is frequently the case for endogenous microRNAs, the Ago2 activity will be stalled and hydrolysis will not occur. Thus, the formation and stability of these stalled complexes and their incorporation into stress granules will alter the local protein population, and in turn, functional properties of the cell.

The mechanisms through which environmental changes are communicated into the cell to promote stress granule formation are unclear and likely to differ with different types of stress. Here, we show that extracellular signals can impact stress granule formation via G proteins to reduce the production of specific proteins. Signaling through G proteins is initiated when external ligands bind to their target G protein coupled receptor that activates intracellular Gα subunits. The Gαq family of G proteins is activated by agents such as acetylcholine, dopamine, bradykinin, serotonin, histamine, etc. (*9, 10*). Activated Gαq in turn activates phospholipase Cβ (PLCβ) which catalyzes the hydrolysis of the signaling lipid phosphatidylinositol 4, 5 bisphosphate resulting in an increase in intracellular calcium. While the major population of PLCβ1 lies on the plasma membrane where it binds Gαq and accesses its substrate, PLCβ is also found in the cytosol in every cell type examined and under different conditions (*11, 12*). Several years ago we found that a cytoplasmic PLCβ population binds to C3PO, the promoter of RNA-induced silencing, and this binding can reverse RNA-induced silencing of specific genes (*12, 13*). Reversal of silencing was independent of PLCβ1's catalytic activity. Subsequent studies showed that the association of PLCβ and C3PO is critical for PC12 differentiation (*14, 15*), but little or no association is seen when cells are not differentiating leading to the question of whether cytosolic PLCβ has other binding partners. Recently, we found that PLCβ1 will bind to and inhibit the neuronal proliferation enzyme CDK16 (*16, 17*), and this association is necessary to keep cells in the G1 phase (*15*). Again, this association is confined to proliferating neuronal cells, suggesting that under non-proliferating, non-differentiating conditions cytosolic PLCβ serves some other function. In this study, we show that a major population of cytosolic PLCβ is bound to stress granules proteins, and that this binding prevents premature stress granule formation. Removal of PLCβ1 from the cytoplasm by stress or

by Gαq stimulation promotes stress granule formation. The interaction between PLCβ1 and stress granule proteins shows a novel feedback mechanism between agents in the external environment and the protein translation machinery.

RESULTS

PLCβ1 binds to stress granule-associated proteins. We wanted to determine novel binding partners to cytosolic PLCβ1 under non-differentiating conditions. Our approach was to isolate the cytosolic fractions of unsynchronized (where 90% are in the G1 phase (*15*)), undifferentiated PC12 cells, and pull down proteins bound to PLCβ1 using a monoclonal antibody. The proteins contained in these complexes were identified by mass spectrometry. We find that ~30% of the total proteins associated with cytosolic PLCβ1 are markers for stress granules (*18*). The most prevalent ones are listed in **Fig.1A**.

To see whether the binding of PLCβ1 to stress granule proteins occurs only in unsynchronized cells where ~90% in the G1 phase, we repeated these studies in PC12 cells arrested in the G2/M phase by treatment with nocodazole, and these results are presented in **Fig.1B**. Again, we find that 32% of the proteins bound to PLCβ are markers for stress granules, with the most prominent being eukaryotic initiation factor 5A (eIF5A) and polyadenylate binding protein C1 (PABPC1) (**Fig.1B**). Additionally, other stress-granule and translation proteins appear at high or moderate levels in both groups such as FXR1/2 and other eukaryotic initiation factors. It is also notable that Ago2, which is associated with both RNA-induced silencing complexes and stress granules (*7*), appears in these cells.

To support the mass spectrometry studies, we repeated the pull-down studies and monitored the association of two stress granule proteins by western blotting. The first, PABPC1, is an established marker for stress granules (*18*). The second, Ago2 which moves into granules under stress conditions (*7*). Again, using unsynchronized, undifferentiated PC12 cells, we verified that PABPC1 and Ago2 associated with PLCβ1. We then measured whether these levels changed when two of PLCβ1's established binding partners Gαq and TRAX (C3PO) are over-expressed (Note that PLCβ1 binds to TRAX subunits of C3PO (*19*)). We find (**Fig. 2**) that the level of Ago2 is reduced when either Gαq or TRAX is over-expressed, suggesting that Ago2 binds to similar regions of PLCβ1. However, the amount of PABPC1 pulled down with PLCβ is unchanged with over-expression of either Gαq or C3PO. The simplest interpretation of these data is that interactions between PLCβ and PABPC1 differ from those with Ago2, and that the reduction in PABPC1 levels in Ago2 over-expression is simply due to a redistribution of the PLCβ1 pool (see *Discussion*). Nevertheless, our studies confirm the mass spectrometry studies above and show that cytosolic PLCβ1 associates with stress granules proteins.

Association between PLCβ1 and Ago2 is sensitive to cell conditions. The above studies indicate that interactions between PLCβ and Ago2 may be modulated by G protein stimulation and cellular events associated with C3PO. Keeping in mind that C3PO promotes RNA-induced silencing, we set-out to characterize the factors that regulate PLCβ-Ago2 association. We first

isolated the cytosolic fractions of unsynchronized, undifferentiated PC12 cells, pulled-down proteins associated with Ago2 and identified them by mass spectrometry. We find that PLCβ is included in the set of data. Interestingly, all of the proteins listed in **Fig. 1A** were found in both PLCβ1 and Ago2 pull-downs.

We measured the association between PLCβ1 and Ago2 in living PC12 cells by Förster resonance energy transfer (FRET) as monitored by fluorescence lifetime imaging microscopy (FLIM). In this method, FRET efficiency is determined by the reduction of the time that the donor spends in the excited state (i.e., the fluorescence lifetime) before transferring energy to an acceptor fluorophore (see (*20*)). If we excite the donor with modulated intensity, the lifetime can be determined by the reduction in modulated intensity (M) as well as the shift in phase (φ) of the emitted light. FRET can then be readily determined from the raw data by plotting the lifetimes in each pixel in the image on a phasor plot (i.e. S versus G where S = M*sin (φ) and G = M*cos (φ) (see (*21*)). In these plots, the lifetimes from each pixel in a FLIM image will fall on the phasor arc for a single population, such as eGFP- PLCβ1. However, when two or more lifetimes are present, the points will be a linear combination of the fractions with the points inside the phase arc that move towards the right due to shortened lifetimes (i.e. FRET). We note that phasor representation is simply the Fourier transform of the lifetime decay curves but readily displays lifetimes directly from raw data without the need for model-dependent fitting of the lifetimes or other corrections.

In **Fig. 3** we show the phasor plot and the corresponding image of a PC12 cell expressing eGFP-PLCβ1 where the phase and modulation lifetime of each pixel in the image is presented. As expected for a single lifetime species, all points fall on the phasor arc (**Fig. 3A**). When we repeat this study in cells expressing both eGFP-PLCβ1 and mCherry-Ago2 where mCherry is a FRET acceptor, the average donor lifetime drops from 2.5 to 1.7ns, and the points move inside the phasor (**Fig. 3B**). This reduction in lifetime and movement of the points into the phasor show validates the occurrence of FRET between the probes. Because the amount of FRET depends on the distance between the fluorophores to the sixth power, and since the distance at which 50% transfers for the eGFP / mCherry pair is ~30Å (*22*), our results imply direct interaction between PLCβ1 and Ago2 in the cytosol.

We can select points in the phasor plots and visualize their localization in the cell image. We find that the points indicating FRET, and thus eGFP-PLCβ1 / mCherry-Ago2 complexes, are localized in the cytoplasm (**Fig. 3C**). In contrast, points corresponding eGFP-PLCβ1 alone are found both on the plasma membrane and the cytoplasm.

PLCβ1 binds to eIF5A in the same region as C3PO and Gαq. To remain cytosolic, stress granule proteins must bind to PLCβ1 in a manner competitive with Gαq or they would localize to the plasma membrane. We previously have shown that PLCβ1 binds to C3PO in the same C-terminal region as Gαq (*13*) and that competition between C3PO/Gαq regulates PLCβ1's ability to generate calcium signals through Gαq activation, or to reverse siRNA, respectively (*23*). With this in mind, we searched the proteins identified in the mass spectrometry for stress granule proteins that could draw PLCβ1away from Gαq. These data indicate a strong association between PLCβ1 and eIF5A (**Fig.1**). Additionally, eIF5A, which is a GTP-activating protein (*24*), has homologous regions to the GTPase region of Gαq (see *Discussion*) and so we chose it for further testing.

In an initial study, we purified PLCβ1 and covalently labeled it with Alexa488 that served as a FRET donor. We then purified eIF5A, labeled it with a FRET acceptor, Alexa594, and measured the association between the two proteins in solution similar to previous studies (*25*). We find that the two proteins bind with strong affinity (K_d = 27 ± 5nM). However, when we formed the Alexa488-PLCβ1-C3PO complex and titrated Alexa594-eIF5A into the solution, we could not detect FRET. This result suggests that eIF5A binds to the same region as C3PO, and similarly, to Gαq (see (*13*)).

To determine whether eIF5A competes with C3PO for PLCβ1 in cells, we transfected PC12 cells with eGFP-PLCβ1 and mCherry-TRAX, the main binding subunits of C3PO (*19*). Association between these proteins is easily detected by FLIM/FRET (**Fig. 4A-B**). We then microinjected purified eIF5A to increase its intracellular amount by ~10nM and find that FRET is completely eliminated (**Fig. 4C**). This results shows that eIF5A displaces C3PO from PLCβ1 and suggests that both proteins bind to a similar region in PLCβ1's the C-terminus. To confirm this idea, we formed the eIF5A-PLCβ1 complex, chemically cross-linked proteins, digested the samples, electrophoresed and identified the bands by mass spectrometry. We find several interaction sites between the proteins including residues 1085-1095 of PLCβ1and 97-103 of eIF5A which are expected to be close to the Gαq activation region. Taken together, these studies suggest that eIF5A acts of the primary interaction site between PLCβ1 and other stress granule proteins, and competes with both Gαq and C3PO for PLCβ1 binding.

Effect of osmotic stress on PLCβ1 isoforms. To determine whether PLCβ1 can impact stress granule formation, we started with mild, hypo-osmotic stress (300 to 150 mOsm) that some cells may experience under normal physiological conditions and where we have found has reversible effects on the Gαq/PLCβ signaling pathway in muscle cells (*26, 27*). It is probable that osmotic stress would produce stress granules that are different in size, number and composition from the well-studied structures produced by $NaAsO_2$. We measured changes in the association between PLCβ1 and stress granule proteins under hypo-osmotic stress. In these experiments, the osmolarity was reduced from 300 to 150 mOsm for 5 and 33 minutes. We focused on initial (i.e. 5 minutes) stress effects before adaptive changes in the cell occur.

PLCβ1 has two major subtypes (1a and 1b) where the 1a form has additional residues in its C terminus (1142-1216) (*28*). PLCβ1a is the most prevalent subtype and is the isoform used here in pull-down studies (i.e. mass spectrometry and western blottin), down-regulated by siRNA, and expressed as an eGFP fusion. We note that some studies found that the deletion in the 1b sequence affects the cellular localization and these changes differ in different cell types (*29-31*). We determined how osmotic stress affected the cellular levels of the two PLCβ1 isoforms. As a control, we verified that the levels of the two isoforms were unchanged with Gαq stimulation. When we subjected cells to hypo-osmotic stress for 5 minutes, we find that the PLCβ1a isotype is eliminated (**Fig. 5A**). Tracking the levels of PLCβ1 microscopically, we quantified this loss in the cytosolic population (**Fig. 5B**). Considering the half-time of PLCβ1a in PC12 cells is 20 min (*15*), this result suggests that osmotic stress enhances PLCβ1a degradation. This loss of PLCβ1 is seen by ablation of calcium signals transduced through Gαq / PLCβ1 when cells are under osmotic stress (**Fig. 5C**). After 30 min of stress, the level of PLCβ1b increases as does the level of

PABPC1, but PLCβ1a remains low as the cells recover increases suggesting that these proteins play a part in adaptive responses (**Fig. 5B**).

Cytosolic levels of PLCβ1 impact stress granule assembly. It is possible that PLCβ1 binds stress granule associated proteins to prevent premature assembly of stress particles. To test this idea, we followed stress granule formation in PC12 cells under hypo-osmotic stress by counting the number of particles microscopically in undifferentiated, unsynchronized PC12 cells using a 100x objective under normal (300 mOsm) and hypo-osmotic conditions (150 mOsm). We note that this resolution may not capture the formation of small particles (see (*4*)) and we might be viewing the assembly of primary particles as well as the fusion of small pre-formed ones. We also note that we analyzed particle number and sizes in 1.0 μ slices though several cells as noted in the figures. Therefore, we report particle sizes in area as seen for each slice since converting the particles into three dimensions would result in a loss in resolution and was not necessary for this analysis.

We fixed PC12 cells under normal and hypo-osmotic conditions and stained them with monoclonal antibodies to the stress granule marker, PABPC1. In control cells, PABPC1 antibody staining shows ~750 particles below 25 μm^2 (**Fig. 6A**). When PLCβ1 is down-regulated, we find a large increase in PABPC1 particles from 25 to 100 μm^2 suggesting that PLCβ1 is promoting the formation of larger particles. When we apply osmotic stress we find an increase in the number of particles between 25 and 50 μm^2 (**Fig. 6B**) However, osmotic stress does not change the size or number of particles in cells where PLCβ1 has been down-regulated suggesting that osmotic stress and loss of PLCβ1 are not additive effects. In another series of studies, we stimulated cells with carbachol to activate Gαq (**Fig. 6C**). We find that stimulation produces a high number of particles up to ~150 μm^2 and down-regulating PLCβ1 does not greatly impact the size or number of PABPC1 particles. Taken together, these studies suggest that loss of PLCβ either from down-regulation, osmotic stress or binding to activated Gαq promotes the incorporation of PABPC1 into larger aggregates.

We then tested the effect of PLCβ1 levels on particles associated with Ago2 by immunofluorescence. For this protein, the number of smaller particles substantially increased when PLCβ1 was down-regulated (**Fig. 7A**). Unlike PABPC1, the size and number of Ago2-associated particles were not affected by osmotic stress, although an increase in the number of small particles with PLCβ1 down-regulation was still seen (**Fig.7B**). Additionally, carbachol stimulation of Gαq resulted in a number in the number of small particles (**Fig.7C**) We also viewed Ago2 particle association by transfecting PC12 cells with mCherry-Ago2 and monitoring the formation of particles in real time (**Fig. 7D**). While the number and areas varied somewhat with the level of transfection, the results show the same trend as for the immunostained samples. Thus, reduction of cellular PLCβ1 results in a large number of smaller Ago2-associated particles.

While the increase in PABPC1 and Ago2 particle assemblies could simply be due to the loss of cellular PLCβ1, it may also be due to removal of PLCβ1 from pre-formed particles. To address this question, we transfected PC12 cells with eGFP-PLCβ1 and analyzed the particles (**Fig.7E**). We could not detect particles below 400 μm^2 after which the number climbed to ~1000. No changes occurred with osmotic stress. These data suggest that PLCβ1 does not associate with large

particles in the cell and correlates well with fluorescence correlation studies showing that diffusion of eYFP-PLCβ1 is unchanged at 4.2 +/-0.4 $\mu m^2/s$ (*not shown*).

The differences in the size and number of PABPC1 and Ago2 particles suggest they partition into different aggregates. We tested this idea by monitoring the effect of PLCβ1 and osmotic stress on the colocalization between Ago2 and PABPC1 (**Fig. 8**). Under normal osmolarity, we find little colocalization between the proteins both at endogenous and knocked-down levels of PLCβ1. However, when the cells are subjected to osmotic stress, colocalization between the species increases, and this increase is more pronounced when PLCβ1 is down-regulated. Increased colocalization may be due to a greater number of both PABPC1 and Ago2 associated particles in the cytoplasm due to loss of cytosolic PLCβ1.

Assembly of Ago2 stress granules depends on the environmental stress. We followed the formation of Ago2-associated particles by Number & Brightness analysis (see *Methods*). This method measures the number of fluorescent particles associated with a diffusing particle in living cells. By comparing the number of eGFP-Ago2 molecules diffusing in PC12 cells as compared to free eGFP, we can estimate how many eGFP-Ago2 molecules are associated with the diffusing particles. Control PC12 cells showed a uniform distribution of eGFP-Ago2 similar to free eGFP indicating a single eGFP-Ago2 (**Fig. 9A**). Subjecting cells to osmotic stress resulted in non-uniform distribution of eGFP-Ago2 particles (**Fig. 9B**) in which almost 60% of the eGFP-Ago2 were larger than a monomer. However, aggregation of eGFP-Ago2 was not promoted by either cold shock (12ºC for 1 hour), heat shock (40ºC for 1 hour) (**Fig. 9C-D**) or oxidative stress (1mM $CoCl_2$ 8hrs, *not shown*) suggesting that Ago2 only incorporates into stress granules under osmotic stress.

Cytosolic PLCβ1 levels impacts the size of cytosolic RNAs. If PLCβ1 is promoting the incorporation of Ago2-associated stress granules, we would expect an increase in the size distribution of cytosolic RNA as mRNA accumulates due to the arrest of translation. We assessed changes in the size distribution of cytosolic RNA by dynamic light scattering **(Fig. 10)**. Subjecting cells to osmotic stress caused a significant shift to larger sizes. Down-regulating PLCβ1 resulted in a small peak at low molecular weights followed by a broad peak at larger sizes that shifts to the right when compared to control. The small peak is consistent with enhanced C3PO activity due relief of inhibition by PLCβ1 (*25*). . Over-expressing Gαq resulted in a similar behavior as siRNA (PLCβ1). Surprisingly, neither cold, heat or oxidative stress (not shown) increased the average size of cytosolic RNA. These data are consistent with the translation arrest and accumulation of higher molecular weight RNAs due to Ago2-associated particles when the cellular level of PLCβ1 is reduced.

Cytosolic PLCβ1 levels affect stress granules in smooth muscle cells. Myocytes and other cell types may experience changes in osmotic conditions during their lifetime. With this in mind, we extended these studies to a rat aortic smooth muscle line (A10). We initially carried out mass spectrometry studies on cytosolic PLCβ1 complexes in A10 cells. We find PLCβ1 binds to a number of stress granules proteins and many of these were also found in PC12 cells, e.g. PABPC1 and eIF5A. Some stress granule proteins, such as Ago2 and FXR are not seen (**Fig. 11A**). When

we repeated this study in cells subjected to osmotic stress for 5 minutes, a very different set of proteins bound to PLCβ1. Almost no stress-granule proteins were seen, and the few that were found differed greatly from the control (**Fig. 11B**). These results show that PLCβ1 binds to stress granule associated proteins in A10 as well as PC12 cells, and that osmotic stress releases these proteins from PLCβ1. We note that like PC12 cells, the cellular amount of PLCβ1a in A10 cells is reduced with osmotic stress and unchanged with carbachol stimulation.

We measured the formation of PABPC1 particles when the cytosolic levels of PLCβ1 are perturbed, i.e. osmotic stress, siRNA down-regulation and Gαq stimulation (**Fig. 11C-E**). These cells showed particles that are ~10 fold larger than in PC12 cells. The lower expression of PLCβ1 in A10 cells along with absence of FXR1/2 and other neuronal specific proteins maybe reflected in our inability to detect small particles associated with PABPC1. Like PC12 cells, down-regulating PLCβ1 resulted in larger particles, and osmotic stress increased the formation of large particles that become smaller when PLCβ1 is down-regulated. Carbachol stimulation results in a significant increase in particle formation. In summary, these studies show that the size and number of PABPC1 particles depend on the cytosolic level of PLCβ1.

Dependence of stress granule formation on PLCβ1 levels. To understand the dependence of stress granule formation on the concentration of PLCβ, we assume that eIF5A is the primary contact between PLCβ1 and stress granule proteins. We can then express the partitioning of eIF5A from the cytosol (c) to the particulate phase (p) as:

$$Kp = \frac{eIF5A^{p}}{eIF5A^{c}}$$

where $eIF5A^{p}$ is the stress granule phase also termed '*G'*. The total amount of eIF5A is:

$E_T = eIF5A^{p} + eIF5A^{c}$, where $eIF5A^{c} = eIF5^{free} + eIF5A\text{-}PLC\beta$

We can express the association between PLCβ and eIF5A in terms of a bimolecular dissociation constant.

$$K_d = \frac{[PLC\beta][eIF5A]}{[PLC\beta - eIF5A]}$$

In this equation, PLCβ refers to cytosolic PLCβ. We only consider the cytosolic population and not the membrane-bound one in accord with our results showing that loss of cytosolic of PLCβ promotes stress granule formation. Thus, the total cytosolic amount of PLCβ is:

$P_T = PLC\beta^{free} + PLC\beta\text{-}eIF5A$

If we combine these equations to determine the relationship between and [PLCβ], we obtain an equation that is quadratic in *G* (i.e. $eIF5A^{p}$.

$$G^2\left(1+\frac{1}{K_p}\right)+G\left(P_T-E_T+K_pK_d+K_d\right)-K_pK_dE_T=0$$

To give:

$$G=\frac{-\left(P_T-E_T+K_d\left(1+K_p\right)\right)\pm\sqrt{P_T^2+E_T^2+K_d^2\left(1+K_p\right)^2+2K_d\left(1+K_p\left(P_T+E_T\right)\right)-2P_TE_T}}{\left(\frac{2\left(1+K_p\right)}{K_p}\right)}$$

To determine the applicability of this model, we first need to estimate values for *G*. We find a linear dependence between the number of particles and the average area of the particles for PABPC1 (**Fig. 12A-B**) in both PC12 or A10 cells. This linearity allows us to estimate *G* using either of these measurements. We note that this linearity does not occur for Ago2 particles where stress primarily increases the number of particles rather than the size (**Figs. 6-7**).

We can estimate the total amount of cytosolic PLCβ using single molecule fluorescence measurements that, after calibration, determine the number of eYFP-PLCβ1 molecules diffusing in a specific confocal volume, and we note that we typically over-express ~2 fold more protein as indicated by western blotting. Our measurements give a cytosolic eYFP-PLCβ1 concentration of ~43 nM in PC12 cells and ~49nM in A10 cells which is reduced to 10-15 nM under hypo-osmotic conditions. This decline can be compared with the ~2.5 fold reduction in cytosolic PLCβ upon carbachol stimulation (e.g. **Fig. 5B**) and the 80-90% reduction in PLCβ1 levels with siRNA treatment. Although these values for PLCβ1 are very approximate, we can use them to determine its dependence on stress granules as expressed as G^2. The data in **Fig. 12C** show the sensitivity of stress granules in this concentration range of PLCβ1 (see *Discussion*)

DISCUSSION

In this study, we show that the atypical cytosolic population of PLCβ1a helps to organize Ago2-associated stress granules in response Gαq signals or under osmotic, but not cold, heat or oxidative stress. PLCβ1 plays an important but unknown role in neuronal development. We have found that the expression of PLCβ1a increases dramatically within the first 24 hrs of PC12 cells differentiation and decreases after (*14*) leading to the question of why its expression is so variable. As detailed below, our studies suggest that PLCβ1 regulates the entry of Ago2, PABPC1 and other stress granule proteins into particulates through simple thermodynamic binding mechanism that is competitive with Gαq, and that is absolutely dependent on the cytosolic level of PLCβ. We propose that cells use cytosolic PLCβ1 levels to regulate the formation and timing of protein synthesis, and to prevent the formation of irreversible aggregates.

The traditional function of PLCβ is to generate calcium signals through molecules that activate Gαq such as acetylcholine, dopamine, serotonin, and melatonin. However, it is clear that PLCβ1 plays multiple roles in cell function. Cocco and other have shown that PLCβ1 can localize to the

nucleus to regulate cell growth and differentiation (see (*32, 33*)). Our lab has found that PLCβ1 has a stable cytosolic population that impacts various cell functions, such as RNA silencing, and neuronal cell differentiation and proliferation (*34, 35*). These alternate cytosolic functions of PLCβ only occur at specific and limited times in the cell cycle. For this reason, we set out to determine whether PLCβ1 binds to other partners in non-differentiating cells under non-stimulated conditions. Using a proteomics approach, we found that PLCβ1 associates with stress granule proteins.

Stress granules are RNA/protein aggregates that allow cells to halt protein translation of non-essential proteins. We find that many of the proteins that associate with PLCβ1 complexes directly contribute to RNA processing and ribosome assembly; and these proteins are found in PLCβ1 complexes isolated from PC12 cells as well as A10 cells. Initiation of protein translation begins with the binding of PABP to the polyadenylate tail of mRNA which is followed by the association of eukaryotic initiation factors (*36*). A cytosolic from of PABP, i.e. PABPC1, was found in our PLCβ1 pull-downs, along with eIF4 subtypes, which can bind to PABPC1 (see https://www.uniprot.org/uniprot/P11940). Several other eukaryotic initiation factors were also identified in our analysis.

Progression of translation proceeds by hydrolysis of GTP on eIF2 which is catalyzed by the GTPase activity of eIF5, and our results indicate that eIF5A may be the primary binding partner for PLCβ1 association with stress granule proteins. EIF5A is prominent in PLCβ1 pull-downs and has several regions in its sequence that are homologous to Gαq including a region where Gαq directly contacts PLCβ (aa 147-162) as indicated by homologous sequence alignment and chemical cross-linking (see (*37*)). We directly tested the association between PLCβ1 and eIF5A. Not only was the PLCβ1-eIF5A affinity in the same range as the affinity between PLCβ1 and C3PO (*13*) but binding was competitive both in solution and in cells. Because the binding site of C3PO overlaps the binding site of Gαq, then PLCβ1 association with eIFA will depend on the level of Gαq activation and this behavior is indicated in our results. Thus, in the absence of Gαq stimulation, a major population of cytosolic PLCβ1 associates to eIF5A until events, such as differentiation causes PLCβ1 binding to shift to C3PO and inhibit of RNA-induced silencing.

We find that population PLCβ1 also binds to Ago2 as seen in pull-down studies, co-immunoprecipitation and FRET/FLIM . Our ability to disrupt their interactions by the addition of purified eIF5A suggest that it is a primary association. Ago2 is the key nuclease component of the RNA-induced silencing complex (RISC) (see (*38*)) and our previous hinted an association between these enzymes (*12*). Sequence alignment of Ago2 and the TRAX subunits of C3PO shows four homologous regions ranging from ~20-40 aa in length and from 21-30% identity and 40-56% homology (2-54, 87-119, 202-228, 109-136 on C3PO and 788-826, 555-598, 188-202, 831-858 Ago2). It is notable that at least three of the TRAX regions are potential interaction sites for PLCβ1 binding and at least one of these may be available for PLCβ1-Ago2 binding (*25*). By this argument, it is possible that PLCβ1 directly binds Ago2 through similar interactions as TRAX.

Since PLCβ1 associates with PABPC1 and Ago2, we were curious to determine whether its presence impacts stress granule formation. We chose mild osmotic stress that may occur in some cells under certain physiological conditions. The acute and mild osmotic some cells are routinely subjected to and easily handled physiologically. Hypo-osmotic stress initiates a series of cellular events to reduce the number of osmolytes in the cell, such as the synthesis of glycogen

from glucose, and as well as ion flow (*39*). We were surprised to find a large reduction in PLCβ1a throughout the cell when osmotic stress is initially applied. PLCβ1a and 1b isoforms differ by ~20 amino acids in the C-terminal region. Cocco and colleagues have found that PLCβ1b, but not PLCβ1a, prevents cell death under oxidative conditions by impacting levels of key signaling proteins (*40*). Additionally, PLCβ1 and 1b may localize differently depending on the cell types (*28-31, 41, 42*) although our imaging studies suggest this is not the case in PC12 cells where the two proteins are similarly distributed in the cell. At this point, the mechanism that preferentially degrades PLCβ1a as opposed to PLCβ1b under osmotic stress is unclear, but does not occur under cold or heat shock (*unpublished*). In any case, the reduction in cytosolic PLCβ1a was one of three methods we used to understand its affect in the formation of particles associated with PABPC1 and Ago2; the other two methods were stimulation of Gαq to drive PLCβ1 to the plasma membrane, and treatment with siRNA(PLCβ1a). All these methods showed that removal of cytosolic PLCβ1 affects promotes the formation of particles.

We monitored the appearance of stress granules under hypo-osmotic conditions structurally by fluorescence imaging and functionally by the accumulation of large cytosolic RNAs. Parker and colleagues have shown that initially, stress granules are small and grow in size in a time-dependent manner (*4*). Here, we resolved particles over 10 μ^2 that form in the cytoplasm and we note that the size and number of particles did not vary between 5 and 10 minutes after induction of stress. Additionally, while a very small population of eGFP-PLCβ1 incorporated into particles ~400 μ^2 these were unchanged with osmotic stress suggesting that PLCβ1 delivers proteins into particles but does not incorporate. PABPC1 was associated with a high number of aggregates whose numbers were affected by the level of cytosolic PLCβ1a as determined by immunofluorescence. Formation of Ago2-associated particles, as monitored by both immunofluorescence and in live cell imaging, was sensitive to Gαq stimulation and other but not other stresses. Importantly, our data suggest that cells respond to Gαq activation by sequestering Ago2 into stress granules to halt the production of specific proteins.

Our studies indicate that Gαq activation promotes the formation of Ago2-associated stress responses through PLCβ1, and this some mechanism occurs for cells subjected to osmotic stress where a loss of PLCβ1a is observed. It is notable that cold, heat or oxidative stress does not result in Ago2 aggregation and does not significantly affect the sizes of cytosolic RNAs even though we have shown that oxidative stress greatly reduces PLCβ1 (*43*). These results suggest that the type of stress controls the composition of stress granules including the amount of mRNA-Ago2 complexes.

A loss in cytosolic PLCβ1 may arrest the translation of specific proteins by promoting the formation of mRNA-Ago2-associated stress granules. In a preliminary study, we monitored the levels of Hsp90A with PLCβ1 down-regulation. Hsp90A is heat inducible with a complex set of regulation mechanisms (*44*). We choose Hsp90 because it does not appear to be strongly regulated by PLCβ1-C3PO (*12*) and because its transcripts may be associated with stress granules formed by arsenite exposure stress (*45*). Western blotting shows a reduction in Hsp90 levels with siRNA(PLCβ1) by as much as ~6-fold consistent with increased formation of Ago2-associated stress granules. The idea that sustained Gαq activation can regulate the production of specific proteins is intriguing and a comprehensive study of all of the transcripts affected by PLCβ1 is now underway.

Neurons and cardiomyocytes are long-lived cells and their health depends on reversible assembly of stress granules. We used PC12 cells as model for the role of stress granules in neurological diseases and A10 cells as a model for muscle cells regularly handle changes in osmolarity. We were pleased to find a similar set of stress related proteins in PLCβ1 complexes in the two cell lines with the exception of neural specific proteins and RNA-induced silencing proteins (i.e. Ago2 and C3PO). Thus, PLCβ1 may serve a similar in many cell types by mediating stress granule formation but not in regulating RNA processing.

We constructed a simple thermodynamic model in which the partitioning of eIF5A into particulates is regulated by its association with PLCβ1 but note that eIF5A can easily be replaced with Ago2. The expression derived from this model shows the scope that PLCβ1 impacts stress granule formation. Specifically, if the total amount of eIF5A is much higher than PLCβ1, then stress granule formation will be independent of PLCβ1. Considering the high concentration of ribosomes in cells, it is quite likely that eIF5A binding to PLCβ1 is occluded by its associated proteins is high but most likely its association region with PLCb1 is occluded by other interactions. The idea is supported by our microinjection studies showing that delivering ~10nM of eIF5A into cells can displace C3PO from PLCβ1. Regardless of the specific nature of eIF5A and its associated proteins, our data show that there is a concentration range of PLCβ1 that is sensitizes cells to stress granule formation and that this range is under the control of Gαq activation. Additionally, endogenous levels of PLCβ1 help to control premature stress responses.

Stress granule dysfunction has been associated with neuronal cells (see (*46, 47*)) and our particle analysis data as well as DLS studies suggest that PLCβ1 may act as a chaperone to keep stress granule proteins disperse under basal conditions. It is notable that PLCβ1 is highly expressed in neuronal tissue (*48*) and reduced levels are associated with a host of neurological disorders that may result from disruptions in calcium signaling, neuronal cells proliferation and differentiation (e.g. (*49-52*). Schizophrenia and suicide has been shown to specifically involve varying levels of PLCβ1a and 1b in the prefrontal cortex (*51*). It is also notable that the PLCβ1-associated proteins identified here play important roles in neuronal function. FXR proteins are associated with the most common form of hereditary mental retardation (see (*53, 54*)) while eIF5A is associated with neuronal growth and brain development (*55*). It is interesting to speculate connections between PLCβ1 neurological disorders and those associated with FXR and eIF5Awhich may involve dysfunction in stress granule assembly / disassembly.

MATERIALS AND METHODS

Cell culture: PC12 cells were cultured in high glucose DMEM (GIBCO) with 10% heat-inactivated horse serum (GIBCO) and 5% fetal bovine serum (Atlanta Biologicals). A10 cell lines were cultured in high glucose DMEM with 10 % fetal bovine serum. All cells were incubated at 37°C in 5% CO_2.

Cells were synchronized in the G2/M phase as described (*15*). Briefly, 2mM thymidine was added to cells for 24 hours, the medium was removed and replaced by fresh complete culture medium for 8 hours after, 40 ng/ml nocodazole was added.

Plasmids: EGFP-hAgo2 was purchased from (Addgene plasmid # 21981) and was prepared in the laboratory of Philip Sharp (MIT). MCherry-Ago2 was a gift from Alissa Weaver (Vanderbilt University). MCherry-TRAX-C1 plasmid was constructed by inserting TRAX gene between BamHI and EcoRI restriction sites in mCherry-C1 backbone using T4 DNA ligase (NEB). Plasmid transfections and siRNA knock-downs were done using Lipofectamine 3000 (Invitrogen) in antibiotic-free media. Medium was changed to one containing antibiotic (1% Penicillin/Streptomycin) 12-18 hours post-transfection. For every FLIM experiment, two separate samples were prepared: donor alone, donor in presence of acceptor.

Co-immunoprecipitation: PC12 cells were lysed in buffer containing 1% Triton X-100, 0.1% SDS, 1x protease inhibitor cocktail and 10 mM Tris, pH 7.4. After 200 µg of soluble protein was incubated with 2 µl of PLCβ1/Ago2 antibody overnight at 4 °C. After addition of 20 mg of protein A-Sepharose 4B beads (Invitrogen), the mixture was gently rotated for 4 h at 4 °C. Beads were washed three times with lysis buffer, and bound proteins were eluted with sample buffer for 5 min at 95 °C. Precipitated proteins were loaded onto two 10% polyacrylamide gel. After SDS-PAGE one gel was transferred to nitrocllulose membranes, proteins were detected by immunoblotting with anti-PLCβ1 (D-8, Santa Cruz) and anti-Ago2 (Abcam) antibody.

FRET studies between purified PLCβ1 and eIF5A: PLCβ1 was purified by over-expression in HEK293 cells as previously described, see (*19*). Purification of eIF5A was based on the method described in (*24*). Purified eIF5A in a pET28-mhl vector was expressed in bacteria (Rosetta 2 DE3 plysS) by inoculating 100 mL of overnight culture grown in Luria-Bertani medium into a 2L of Terrific Broth medium in the presence of 50 µg/mL kanamycin and 25 µg/mL chloramphenicol at 37°C. When OD 600 reached ~3.0, the temperature of the medium was lowered to 15°C and the culture was induced with 0.5 mM IPTG. The cells were allowed to grow overnight before harvesting and stored at -80°C. Frozen cells from 1.8L TB culture were thawed and resuspended in 150 mL lysis Buffer (20 mM HEPES pH 7.5, 300 mM NaCl, 5% glycerol, 2mM BME, 5mM imidazole, 0.5% CHAPS, protease inhibitor cocktail, 5 µL DNAase) and lysed using a panda homogenizer. The lysate was centrifuged at 15,000 rpm for 45 minutes, added to a cobalt column in binding (20 mM HEPES pH 7.5, 300 mM NaCl, 5% glycerol, 2mM BME, 5mM imidazole), equilibrated in a 4 x 1 mL 50% flurry of cobalt resin, passed the 150 ml of supernatant through each cobalt column at approx.. 0.5ml/min, washed with (1) 20 mM HEPES pH 7.5, 300 mM Knack, 5% glycerol, 2mM BME, 30 mm imidazole, and then (2) 20 mM HEPES pH 7.5, 300 mM NaCl, 5% glycerol, 2mM BME, 75 mM imidazole and eluted with 20 mM HEPES pH 7.5, 300 mM NaCl, 5% glycerol, 2mM BME, 300mM imidazole.

Protein association was assessed by FRET using sensitized emission. Briefly, PLCβ1a and eIF5A were covalently labeled on their N-terminus with Alexa488 and Alexa594 (Invitrogen), respectively, and the increase in acceptor emission when exiting at the donor wavelength in the presence of Alexa488-PLCβ1 was noted. Studies were repeated using by pre-binding catalytically inactive C3PO with Alexa488-PLCβ1.

Mass Spectrometry: Mass spectrometry measurements were carried out as previously described at the University of Massachusetts Medical School (*56*). Cytosolic fractions were isolated from cells, and proteins bound to monoclonal anti-PLCβ1a (Santa Cruz, D-8) were separated by electrophoresis. Proteins were isolated by cutting the gels into 1x1 mm pieces, placed in 1.5 mL eppendorf tubes with 1mL of water for 30 min. The water was removed and 200µl of 250 mM ammonium bicarbonate was added. Disulfide bonds were reduced by incubating with DTT at 50°C for 30 min followed by addition of 20 µl of a 100 mM iodoacetamide 30 min at room temperature. The gel slices were washed 2 X with 1 mL water aliquots. The water was removed and 1mL of 50:50 (50 mM ammonium bicarbonate: acetonitrile) was placed in each tube and samples were incubated at room temperature for 1hr. The solution was then removed and 200 µl of acetonitrile was added to each tube at which point the gels slices turned opaque white. The acetonitrile was removed and gel slices were further dried in a Speed Vac (Savant Instruments, Inc.). Gel slices were rehydrated in 100 µl of 4ng/µl of sequencing grade trypsin (Sigma) in 0.01% ProteaseMAX Surfactant (Promega): 50 mM ammonium bicarbonate. Additional bicarbonate buffer was added to ensure complete submersion of the gel slices. Samples were incubated at 37 C for 18 hrs. The supernatant of each sample was then removed and placed in a separate 1.5 mL eppendorf tube. Gel slices were further extracted with 200 µl of 80:20 (acetonitrile: 1% formic acid). The extracts were combined with the supernatants of each sample. The samples were then completely dried down in a Speed Vac.

Tryptic peptide digests were reconstituted in 25 µL 5% acetonitrile containing 0.1% (v/v) trifluoroacetic acid and separated on a NanoAcquity (Waters) UPLC. In brief, a 2.5 µL injection was loaded in 5% acetonitrile containing 0.1% formic acid at 4.0 µL/min for 4.0 min onto a 100 µm I.D. fused-silica pre-column packed with 2 cm of 5 µm (200Å) Magic C18AQ (Bruker-Michrom) and eluted using a gradient at 300 nL/min onto a 75 µm I.D. analytical column packed with 25 cm of 3 µm (100Å) Magic C18AQ particles to a gravity-pulled tip. The solvents were A, water (0.1% formic acid); and B, acetonitrile (0.1% formic acid). A linear gradient was developed from 5% solvent A to 35% solvent B in 90 minutes. Ions were introduced by positive electrospray ionization via liquid junction into a Q Exactive hybrid mass spectrometer (Thermo). Mass spectra were acquired over m/z 300-1750 at 70,000 resolution (m/z 200) and data-dependent acquisition selected the top 10 most abundant precursor ions for tandem mass spectrometry by HCD fragmentation using an isolation width of 1.6 Da, collision energy of 27, and a resolution of 17,500.

Raw data files were peak processed with Proteome Discoverer (version 2.1, Thermo) prior to database searching with Mascot Server (version 2.5) against the Uniprot_Rat database Search parameters included trypsin specificity with two missed cleavages or no enzymatic specificity. The variable modifications of oxidized methionine, pyroglutamic acid for N-terminal glutamine,phosphorylation of Serine and Threonine, N-terminal acetylation of the protein, and a fixed modification for carbamidomethyl cysteine were considered. The mass tolerances were 10 ppm for the precursor and 0.05Da for the fragments. Search results were then loaded into the

Scaffold Viewer (Proteome Software, Inc.) for peptide/ protein validation and label free quantitation.

Fluorescence correlation (FCS) and N&B measurements—FCS measurements were performed on the dual-channel confocal fluorescence correlation spectrometer (Alba version 5, ISS Inc.) equipped with avalanche photodiodes and a Nikon Eclipse Ti-U inverted microscope as previously described (*27*). For N&B (see (*57*)), we collected ~100 PC12 cell images viewing either free eGFP (control) or eGFP-Ago2, at a 66nm/pixel resolution and at a rate of 4 µs/pixel. Regions of interest (256x256 box) were analyzed from a 320x320 pixel image. Offset and noise were determined from the histograms of the dark counts performed every two measurements. Data were analyzed using SimFC (www.lfd.uci.edu) .

Fluorescence lifetime imaging measurements (FLIM)—FLIM measurements were performed on the dual-channel confocal fast FLIM (Alba version 5, ISS Inc.) equipped with photomultipliers and a Nikon Eclipse Ti-U inverted microscope. A x60 Plan Apo (1.2 NA, water immersion) objective and a mode-locked two-photon titanium-sapphire laser (Tsunami; Spectra-Physics) was used in this study. The lifetime of the laser was calibrated each time before experiments by measuring the lifetime of Atto 435 in water with a lifetime of 3.61 ns (Ref) at 80MHz, 160MHz and 240MHz. The samples were excited at 800/850 nm, and emission spectra were collected through a 525/50 bandpass filter. For each measurement, the data was acquired until the photon count was greater than 300. Fluorescence lifetimes were calculated by allowing ω = 80 MHz:

$$\tau = \frac{S}{G * 2\pi * \omega}$$

Statistical analysis: Data was analyzed using Sigma Plot 13 statistical packages that included student's t-test and one way analysis of variance (ANOVA).

Dynamic light scattering (DLS) — DLS measurements were carried out on a Malvern Panalytical Zetasizer Nano ZS instrument. For these experiments, mRNA from PC12 cells was extracted following the instructions from the Qiagen Mini Kit (Cat #: 74104). Before the mRNA was extracted, cells were exposed to 50% osmotic stress for 5 minutes, treated with siRNA(PLCβ1a), or transfected constitutively-active GαqRC (*58*), and meausred by DLS. For these measurements, approximately 50µL of extracted mRNA in RNase free water was added in a Hellma Fluorescence Quartz Cuvette (QS-3.00mm). Each sample was run 3 times, 10 minutes per run. Control samples were repeated 6 times, PLCβ knockdown twice, and Gαq over-expression once.

Particle analysis — Samples were imaged using a 100X/1.49 oil TIRF objective to microscopically count the number of particles formed under different conditions per μm^2. For each condition, 10-20 cells were randomly selected and z-stack measurements were taken (1.0 µ/frame). Analysis was performed using ImageJ where each measurement was thresholded before analyzing and averaging the number of particles per frame per measurement.

Microinjection studies: Microinjection of a solution of 100 nM eIF5A into PC12 cells was carried out using an Eppendorf Femtojet Microinjector mounted on Nikon Eclipse Ti-U inverted confocal microscope under 0.35 PSI pressure and 0.5 Seconds injection time per injection.

Immunofluorescence: Cells were samples were fixed with 3.7% formaldehyde and permeabilized using 0.1% triton X-100 in PBS then blocked using 10% goat serum, 5% BSA,

50mM glycine in PBS. Cells were then stained with primary antibodies from (Abcam), incubated for 1 hour, washed and treated with a secondary antibody for 1 hour. After another wash, the cells were viewed on either a Zeiss Meta 510 laser confocal microscope. Data were analyzed using Zeiss LSM software and Image J. The secondary antibodies used were Anti-rabbit Alexa-488 for Ago-2 and Anti-mouse Alexa 647 for PABPC1.

Calcium signal Imaging: Single cell calcium measurements were carried out by labeling the cells with Calcium Green (Thermofisher), incubating in HBSS for 45 minutes and washing twice with HBSS. Release of intracellular calcium in live PC12 cells was initiated by the addition of 2 μM carbachol before imaging the time seirs on a Zeiss LSM 510 confocal microscope excitation at 488 using time series mode as previously described, see (*59*).

Western blotting: Samples were placed in 6 well plates and collected in 250μL of lysis buffer that included NP-40 and protease inhibitors as mentioned before, sample buffer is added at 20% of the total volume. After SDS-PAGE electrophoresis, protein bands were transfer to nitrocellulose membrane (Bio-Rad, California USA). Primary antibodies from (Santa Cruz) and (Abcam) are used. Membranes were treated with antibodies diluted 1:1000 in 0.5% milk, washed 3 times for 5 minutes, before applying secondary antibiotic (anti-mouse or anti-rabbit from Santa Cruz) at a concentration of 1:2000. Membranes were washed 3 times for 10 minutes before imaging on a BioRad chemi-doc imager to determine the band intensities. Bands were measured at several sensitivities and exposure times to insure the intensities were in a linear range. Data were analyzed using Image-J.

ACKNOWLEDGEMENTS. The authors are grateful for the support of NIH GM116187. Dr. Garwain is supported by a Richard Whitcomb Fellowship. The authors also would like to thank Dr. Elizabeth Bafaro for her help in cloning mCherry-TRAX and to Dr. Siddartha Yerramilli for help with N&B and for his helpful comments throughout this work.

REFERENCES

1. P. Anderson, N. Kedersha, RNA granules. *J Cell Biol* **172**, 803-808 (2006).
2. D. S. W. Protter, R. Parker, Principles and Properties of Stress Granules. *Trends in Cell Biology* **26**, 668-679.
3. A. Khong *et al.*, The Stress Granule Transcriptome Reveals Principles of mRNA Accumulation in Stress Granules. *Molecular Cell* **68**, 808-820.e805.
4. J. R. Wheeler, T. Matheny, S. Jain, R. Abrisch, R. Parker, Distinct stages in stress granule assembly and disassembly. *eLife* **5**, e18413 (2016).
5. P. Anderson, N. Kedersha, Stress granules. *Current Biology* **19**, R397-R398.
6. M. Ramaswami, J. P. Taylor, R. Parker, Altered Ribostasis: RNA-Protein Granules in Degenerative Disorders. *Cell* **154**, 727-736.
7. A. Detzer, C. Engel, W. Wunsche, G. Sczakiel, Cell stress is related to re-localization of Argonaute 2 and to decreased RNA interference in human cells. *Nucleic Acids Res* **39**, 2727-2741 (2011).

8. S. M. Hammond, A. A. Caudy, G. J. Hannon, Post-transcriptional gene silencing by double-stranded RNA. *Nat Rev Genet* **2**, 110-119 (2001).
9. P. Suh *et al.*, Multiple roles of phosphoinositide-specific phospholipase C isozymes. *BMB reports* **41**, 415-434 (2008).
10. M. Rebecchi, S. Pentylana, Structure, function and control of phosphoinositide-specific phospholipase C. *Physiological Reviews* **80**, 1291-1335 (2000).
11. L. Dowal, P. Provitera, S. Scarlata, Stable association between G alpha(q) and phospholipase C beta 1 in living cells. *J Biol Chem* **281**, 23999-24014 (2006).
12. F. Philip, Y. Guo, O. Aisiku, S. Scarlata, Phospholipase Cβ1 is linked to RNA interference of specific genes through translin-associated factor X. *The FASEB Journal* **26**, 4903-4913 (2012).
13. O. R. Aisiku, L. W. Runnels, S. Scarlata, Identification of a Novel Binding Partner of Phospholipase Cβ1: Translin-Associated Factor X. *PLoS ONE* **5**, e15001 (2010).
14. O. Garwain, S. Scarlata, Phospholipase Cβ-TRAX Association Is Required for PC12 Cell Differentiation. *Journal of Biological Chemistry* **291**, 22970-22976 (2016).
15. O. Garwain, K. Valla, S. Scarlata, Phospholipase Cβ1 regulates proliferation of neuronal cells. *The FASEB Journal* **In press**, fj.201701284R (2018).
16. T. Yanagi, M. Krajewska, S.-i. Matsuzawa, J. C. Reed, PCTAIRE1 Phosphorylates p27 and Regulates Mitosis in Cancer Cells. *Cancer Research* **74**, 5795-5807 (2014).
17. T. Yanagi, S.-i. Matsuzawa, PCTAIRE1/PCTK1/CDK16: a new oncotarget? *Cell Cycle* **14**, 463-464 (2015).
18. H. Mahboubi, U. Stochaj, Cytoplasmic stress granules: Dynamic modulators of cell signaling and disease. *Biochim Biophys Acta* **1863**, 884-895 (2017).
19. S. Sahu, F. Philip, S. Scarlata, Hydrolysis Rates of Different Small Interfering RNAs (siRNAs) by the RNA Silencing Promoter Complex, C3PO, Determines Their Regulation by Phospholipase Cβ. *Journal of Biological Chemistry* **289**, 5134-5144 (2014).
20. J. Lakowicz, *Principles of Fluorescence Spectroscopy, Second Edition*. (Plenum, New York, 1999).
21. M. A. Digman, V. R. Caiolfa, M. Zamai, E. Gratton, The Phasor Approach to Fluorescence Lifetime Imaging Analysis. *Biophysical Journal* **94**, L14-L16 (2008).
22. G. H. Patterson, D. W. Piston, B. G. Barisas, Forster distances between green fluorescent protein pairs. *Anal Biochem* **284** 438-440 (2000).
23. F. Philip, S. Sahu, U. Golebiewska, S. Scarlata, RNA-induced silencing attenuates G protein-mediated calcium signals. *FASEB journal : official publication of the Federation of American Societies for Experimental Biology* **30**, 1958-1967 (2016).
24. F. E. Paulin, L. E. Campbell, K. O'Brien, J. Loughlin, C. G. Proud, Eukaryotic translation initiation factor 5 (eIF5) acts as a classical GTPase-activator protein. *Curr Biol* **11**, 55-59 (2001).
25. S. Sahu *et al.*, Regulation of the activity of the promoter of RNA-induced silencing, C3PO. *Protein Science* **26**, 1807-1818 (2017).
26. Y. Guo, L. Yang, K. Haught, S. Scarlata, Osmotic Stress Reduces Ca2+ Signals through Deformation of Caveolae. *J Biol Chem* **290**, 16698-16707 (2015).
27. L. Yang, S. Scarlata, Super-resolution Visualization of Caveola Deformation in Response to Osmotic Stress. *J Biol Chem* **292**, 3779-3788 (2017).
28. Y. Y. Bahk *et al.*, Two forms of phospholipase C-beta 1 generated by alternative splicing. *Journal of Biological Chemistry* **269**, 8240-8245 (1994).

29. Y. Bahk *et al.*, Localization of two forms of phospholipase Cb1, a and b, in C6Bu-1 cells. *Biochem Biophys Acta* **1389**, 76-80 (1998).
30. C. G. Kim, D. Park, S. G. Rhee, The role of carboxyl-terminal basic amino acids in G_qa-dependent activation, particulate association, and nuclear localization of phospholipase C-b_1. *J Biol Chem* **271**, 21187-21192 (1996).
31. D. R. Grubb, O. Vasilevski, H. Huynh, E. A. Woodcock, The extreme C-terminal region of phospholipase Cbeta1 determines subcellular localization and function; the "b" splice variant mediates alpha1-adrenergic receptor responses in cardiomyocytes. *FASEB journal : official publication of the Federation of American Societies for Experimental Biology* **22**, 2768-2774 (2008).
32. L. Cocco *et al.*, Modulation of nuclear PI-PLCbeta1 during cell differentiation. *Adv Biol Regul* **60**, 1-5 (2016).
33. G. Ramazzotti *et al.*, PLC-beta1 and cell differentiation: An insight into myogenesis and osteogenesis. *Adv Biol Regul* **63**, 1-5 (2017).
34. S. Scarlata *et al.*, Phospholipase Cbeta connects G protein signaling with RNA interference. *Adv Biol Regul* **61**, 51-57 (2016).
35. S. Scarlata, A. Singla, O. Garwain, Phospholipase Cβ interacts with cytosolic partners to regulate cell proliferation. *Advances in Biological Regulation*, (2017).
36. B. Alberts *et al.*, *Molecular Biology of the Cell*. (Garland, New York, 1994).
37. A. M. Lyon *et al.*, An autoinhibitory helix in the C-terminal region of phospholipase C-β mediates Gαq activation. *Nat Struct Mol Biol* **18**, 999-1005 (2011).
38. G. Hutvagner, M. J. Simard, Argonaute proteins: key players in RNA silencing. *Nature Reviews Molecular Cell Biology* **9**, 22 (2008).
39. K. Dietmar, Osmotic stress sensing and signaling in animals. *The FEBS Journal* **274**, 5781-5781 (2007).
40. M. Piazzi *et al.*, PI-PLCβ1b affects Akt activation, cyclin E expression, and caspase cleavage, promoting cell survival in pro-B-lymphoblastic cells exposed to oxidative stress. *The FASEB Journal* **29**, 1383-1394 (2015).
41. A. M. Martelli *et al.*, Nuclear localization and signalling activity of phosphoinositidase C beta in Swiss 3T3 cells. *Nature* **358**, 242-245 (1992).
42. T. M. Filtz, D. R. Grubb, T. J. McLeod-Dryden, J. Luo, E. A. Woodcock, Gq-initiated cardiomyocyte hypertrophy is mediated by phospholipase Cβ1b. *The FASEB Journal* **23**, 3564-3570 (2009).
43. Y. Guo, S. Scarlata, A Loss in Cellular Protein Partners Promotes α-Synuclein Aggregation in Cells Resulting from Oxidative Stress. *Biochemistry* **52**, 3913-3920 (2013).
44. C. Prodromou, Mechanisms of Hsp90 regulation. *Biochemical Journal* **473**, 2439-2452 (2016).
45. A. Khong *et al.*, The Stress Granule Transcriptome Reveals Principles of mRNA Accumulation in Stress Granules. *Molecular Cell* **68**, 808-820.e805 (2017).
46. B. Wolozin, Physiological Protein Aggregation Run Amuck: Stress Granules and the Genesis of Neurodegenerative Disease. *Discovery medicine* **17**, 47-52 (2014).
47. L. Chen, B. Liu, Relationships between Stress Granules, Oxidative Stress, and Neurodegenerative Diseases. *Oxidative Medicine and Cellular Longevity* **2017**, 10 (2017).

48. C. R. Gerfen, W. C. Choi, P. G. Suh, S. G. Rhee, Phospholipase C I and II brain isoenzymes: immunohistochemical localization in neuronal systems in rat brain. *Proc.Natl.Acad.Sci. U.S.A.* **85**, 3208-3212. (1988).
49. A. J. Hannan, P. C. Kind, C. Blakemore, Phospholipase C-β1 expression correlates with neuronal differentiation and synaptic plasticity in rat somatosensory cortex. *Neuropharmacology* **37**, 593-605 (1998).
50. C. E. McOmish, E. L. Burrows, M. Howard, A. J. Hannan, PLC-β1 knockout mice as a model of disrupted cortical development and plasticity: Behavioral endophenotypes and dysregulation of RGS4 gene expression. *Hippocampus* **18**, 824-834 (2008).
51. M. Udawela *et al.*, Isoform specific differences in phospholipase C beta 1 expression in the prefrontal cortex in schizophrenia and suicide. *npj Schizophrenia* **3**, 19 (2017).
52. H.-j. Kim, H.-Y. Koh, Impaired Reality Testing in Mice Lacking Phospholipase Cβ1: Observed by Persistent Representation-Mediated Taste Aversion. *PLOS ONE* **11**, e0146376 (2016).
53. C. Agulhon *et al.*, Expression of FMR1, FXR1, and FXR2 genes in human prenatal tissues. *Journal of neuropathology and experimental neurology* **58**, 867-880 (1999).
54. B. Bardoni, A. Schenck, J.-L. Mandel, The Fragile X mental retardation protein. *Brain Research Bulletin* **56**, 375-382 (2001).
55. Y. Huang, D. S. Higginson, L. Hester, M. H. Park, S. H. Snyder, Neuronal growth and survival mediated by eIF5A, a polyamine-modified translation initiation factor. *Proceedings of the National Academy of Sciences of the United States of America* **104**, 4194-4199 (2007).
56. S. Iwata, Lee, J.W., Okada, K., Lee, J.K. Iwata, M., Rasmussen, B., Link T.A., Ramaswamy, S. and Jap, B.K., Complete at of the 11 subunit bovine mitochondrial cytochrome bc1 complex. *Science* **281**, 64-71 (1998).
57. M. A. Digman, R. Dalal, A. F. Horwitz, E. Gratton, Mapping the Number of Molecules and Brightness in the Laser Scanning Microscope. *Biophys J* **97**, 2320-2332 (2008).
58. T. E. Hughes, H. Zhang, D. Logothetis, C. H. Berlot, Visualization of a functional Gaq-green fluorescent protein fusion in living cells. *J.Biol.Chem.* **276**, 4227-4235 (2001).
59. R. C. Calizo, S. Scarlata, A Role for G-Proteins in Directing G-Protein-Coupled Receptor–Caveolae Localization. *Biochemistry* **51**, 9513-9523 (2012).

FIGURE LEGENDS

1.*Major proteins complexed to PLCβ1 as identified by mass spectrometry*. Proteins associated with PLCβ1 in cytosolic fractions of PC12 cells were pulled down using a monoclonal antibody using **A-** unsyncrhonized cells primarily in the G1 phase, or **B-** PC12 cells arrested in the G2/M phase. All proteins labeled in (**A**) were also identifed in Ago2-associated proteins mass spectrometry studies. Levels of various are expressed as the quantitative normalized iBAQ for each sample. Proteins in red font are phosphorylated bars in blue show cross-matched proteins between PLCβ1 and Ago-2.

2. *Competitive binding of protein partners to PLCβ1*. Compilation of n=8 band (S.D. is shown) intensities from western blotting in co-immunoprecitipiation studies using PLCβ1 as bait. In these studies, changes in the levels of PLCβ1 binding partners (i.e. TRAX (C3PO) and constituatively active Gαq) were identified from cytosolic fractions of untransfected PC12 cells and cells transfected as noted in the graph where PLCβ1 partners were pulled down using a monoclonal antibody.

3. *PLCβ1 binds to Ago2*. Examples of phasor plots in which PC12 cells were transfected with (**A)** eGFP-PLCβ1(A) or (**B)** both eGFP-PLCβ1 and mCherry-Ago2 where the raw lifetimes are plotted as S versus G (see text). Each point in the phasor plots corresponds to the lifetime from the eGFP-PLCβ1 emission seen in each pixel from the corresponding cell image shown in the graph. **C –** a phasor diagrams where the non-FRET and FRET points are selected and the pixels are shown in the cell images.

4. *eIF5A competes with C3PO for PLCβA in cells*. **A -** Example of a phasor plot and the corresponding image from a FLIM measurements of eGFP-PLCβ1a expressed in a PC12 cells. The heat map indicates the eGFP signal intensity. **B -** A similar study as in (**A)** except the PC12 cell is cotransfeted with eGFP-PLCβ1a and mCherry-TRAX(C3PO). Note the movement of pixels into the interior of the phasor arc due to FRET. Purple dots indicates pixels represented in the phasor plot. **C -** The same study as in (**B**) except this cell was microinjected with purifed, unlabeled eIF5A. Note the movement of points back to the phasor arc showing a loss of FRET due to displacement of TRAX from PLCβ1. **D** - Compilation of eGFP-PLCβ1 lifetime results for 2 independent studies wheree n=10 cells each and where a negative control using free mCherry is included. Comparison of data before and after eIF5A microinjection is statistically significant p=<0.001 t-10.665 and f value for Anova test is 96.606.

5. *The effect of osmotic stress on cytosolic PLCβ1.* **A-** A western blot of the cytosolic fractions of PLCβ1 at 300 mOsm under control conditions where PLCβ1a is t the upper band of the doublet and PLCβ1b is the lower band. While the intensities of these band are unchanged 10 minutes after Gαq stimulation with 5μM carbachol, PLCβ1a is not detected at 150 mOsm for 5 and 30 minutes. Lots for PABPC1 and β-tubulin are shown for comparison and n=3. **B** – Results of a study in which eGFP-PLCβ1 was transfected into undifferentiated PC12 cells and changes in cytosolic fluorescence intensity of the middle slice of a z-stack was quantified. Identical behavior was seen over 9 independent experiments, and we note that the plasma membrane population showed similar changes in intensity. **C-** A study showing the change in calcium release when PC12 cells labeled with

Calcium Green are stimulated with 5 µM carbachol under basal conditions (300 mOsm) and hypo-osmotic stress (150 mOsm) where n=12 and SD is shown.

6. *The effect of PLCβ1 on the formation of PABPC1-associated particles in PC12 cells.* The size and number of particles associated with anti-PABPC1 in the cytosol of PC12 cells was measured on a 100x objective and analyzed using Image J (see methods). **A –** Treatment of cells with siRNA(PLCβ1a) results in the formation of larger aggregates relative to mock-transfected controls. An enlarged version of the plot is shown below to allow better comparison. **B-** While osmotic stress (150 mOsm) does not affect the size or number of PABPC1-associated particles, PLCβ1a down-regulated causes a significant increase in particle size and number. **C-** Stimulation of Gαq by treatment with 5 µM carbachol also impacts particle size. All measurements are an average of 3 independent experiments that sampled 10 cells, where SD shown and where the p values was determined using ANOVA.

7. *The effect of PLCβ1 on the formation of Ago2-associated particles in PC12 cells.* In similar study as described above, **t**he size and number of particles associated with anti-Ago2 in the cytosol of PC12 cells was measured on a 100x objective and analyzed using Image J (see methods). **A –** Treatment of cells with siRNA(PLCβ1a) results in the formation of numberous small aggregates relative to mock-transfected controls. **B-** Osmotic stress (150 mOsm) does not affect the size or number of Ago2-associated particles while siRNA(PLCβ1a) causes a significant increase in the number of small aggregates. **C-** Stimulation of Gαq by treatment with 5 µM carbachol results in the formation of a large number of small aggregates and a simialr behavior is observed when PLCβ1 is down-regulated. **D-** Analysis of particles associated with mCherry-Ago2 in live cells under control, 150 mOsm osmotic stress and 5µ carbachol stimulation. **E-** Particles associated with eGFP-PLCβ1a under basal (300 mOsm) and stress (150 mOsm) conditions. For Measurements in **A-C** are an average of 3 independent experiments that sampled 10 cells, while measurements in **D-E** are an average of 3 independent experiments that sampled 5 cells. For **A-E**, SD is shown and the p values were determined using ANOVA.

8. *Change in colocalization of Ago2 and PABPC1 particles with osmotic stress*. **A-** Images of PC12 cells immunstained for Ago-2 (*green*) and PABPC1 (*red*) under (*top to bottom*) basal conditions, when the osmolarity is lowered from 300 to 150 mOsm, when cells are treated with siRNA(PLCβ1) under normal conditions and under osmotic stress. **B-** Graph of the resulting colocalization data were a significant change between 50% osmotic stress sample with wt-PLCβ1 versus siRNA-PLCβ1 samples is noted p=0.002 n=20.

9. *N&B analysis of Ago2 aggregation*. The *top panels* show graphs of the brightness versus intensity with the corresponding cell images in the *bottom panels*. The red box corresponds to monomeric Ago2 while points outside this box and in the green and blue boxes correspond to higher order species. The purple dots in the images denote points sampled in the analysis. **A –** control cells; **B-** cells subjected to hypo-osmotic stress (150 mOsm, 5 min); **C –** cells subjected at cold shock 12ºC for 1 hr; **D –** cells subjected to heat shock at 40ºC for 1 hr.

10. *PLCβ1 levels impacts the size of cytosolic RNAs.* **A-** The size distribution of cytosolic RNA isolated from PC12 cells was measured by dynamic light scattering for control conditions (*black*) and was found to shift to higher sizes with hypo-osmotic stress (150 mOsm 5 min, *green*), over-expression of constituatively active Gαq (*blue*), and down-regulation of PLCβ1 (*pink*). Note that a peak at small RNA sizes is seen for these latter two samples due to reversal of inhibition of C3PO activity by PLCβ1. **B-** An identical study plotting control cells (*black*) cells subjected to hypo-osmotic stress (150 mOsm 5min, *red*), heat shock (40°C for 1 hour, green), cold shock (12ºC for 1 hour, *yellow*). We note that no changes were observed in cells subjected to oxidatiave stress (12 mM $CoCl_2$ 8 hrs) (*not shown*). All peaks were normalized up to 1.0 in order to compare the shifts that occur in the sizes of the cytosolic RNA under different conditions. Each sample was run 3 times, 10 minutes per run. Control samples were repeated 6 times, PLCβ knockdown twice, and Gαq over-expression once.

11. *The effect of PLCβ1 on the formation of PABPC1-associated particles in A10 cells.* Mass spectrometry analysis for proteins associated with PLCβ1 in A10 cells **A-** under normal osmotic conditions and **B-** after 5 minutes of hypo-osmotic stress (150 mOsm). **C-E** The size and number of particles associated with anti-PABPC1 in the cytosol of A10 cells was measured on a 100x objective and analyzed using Image J (*see methods*). **B –** Treatment of cells with siRNA(PLCβ1a) results in the formation of larger aggregates relative to mock-transfected controls. **C -** Osmotic stress (150 mOsm) enhances the formation of PABPC1-associated particles and this behavior is promoted by PLCβ1a down-regulation. **D-** Stimulation of Gαq by treatment with 5 μM carbachol also impacts particle size. All measurements are an average of 3 independent experiments that sampled 10 cells, where SD is shown and p values were determined using ANOVA.

12. *Particle formation is inversely related to PLCβ1 levels*. Relationship between the number of particles and average area of PABPC1 particles found in **A-** PC12 and **B-** A10 cells. C-shows the inverse relationship of the number of particles and the estimated concentraiotn of total cytosolic PLCβ1.

Fig. 1

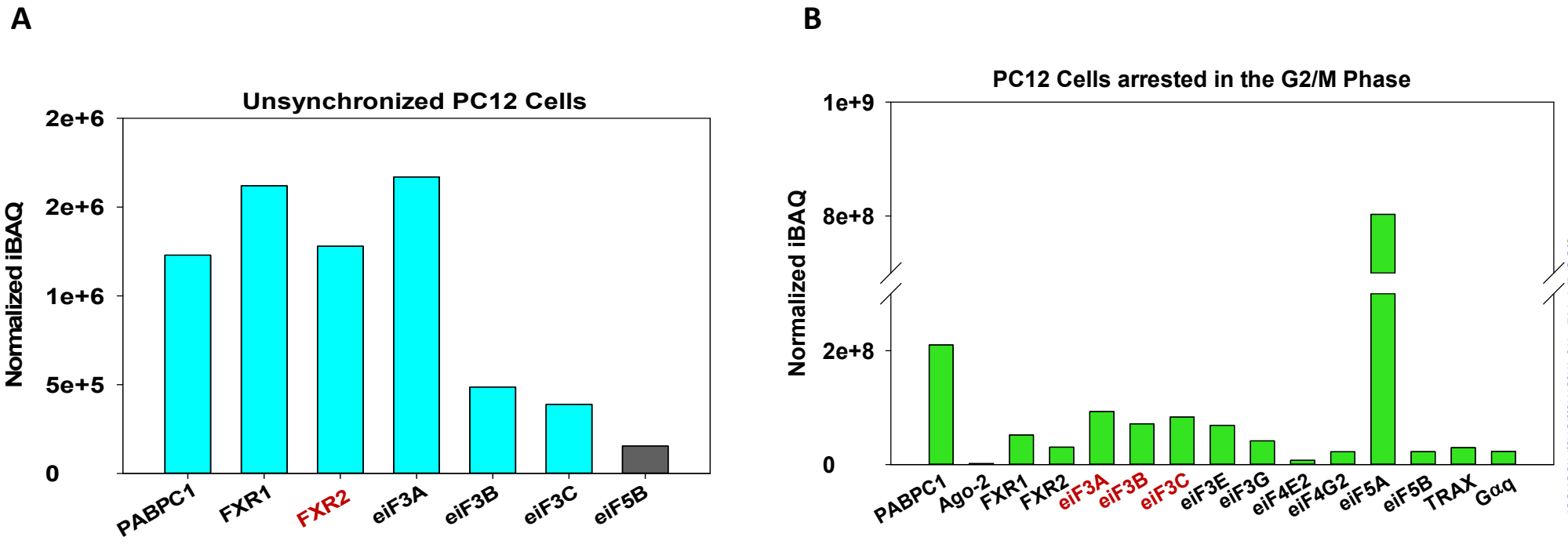

Fig. 2

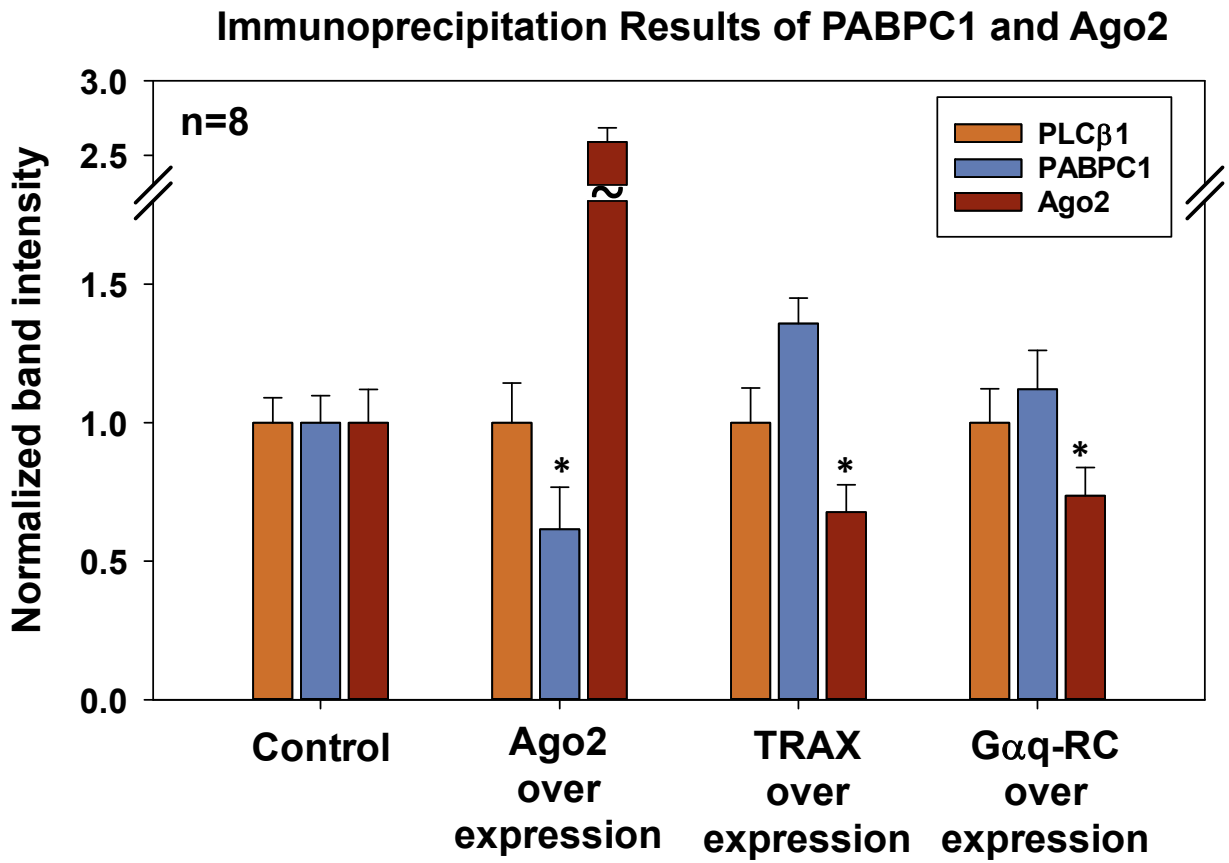

Figure 3

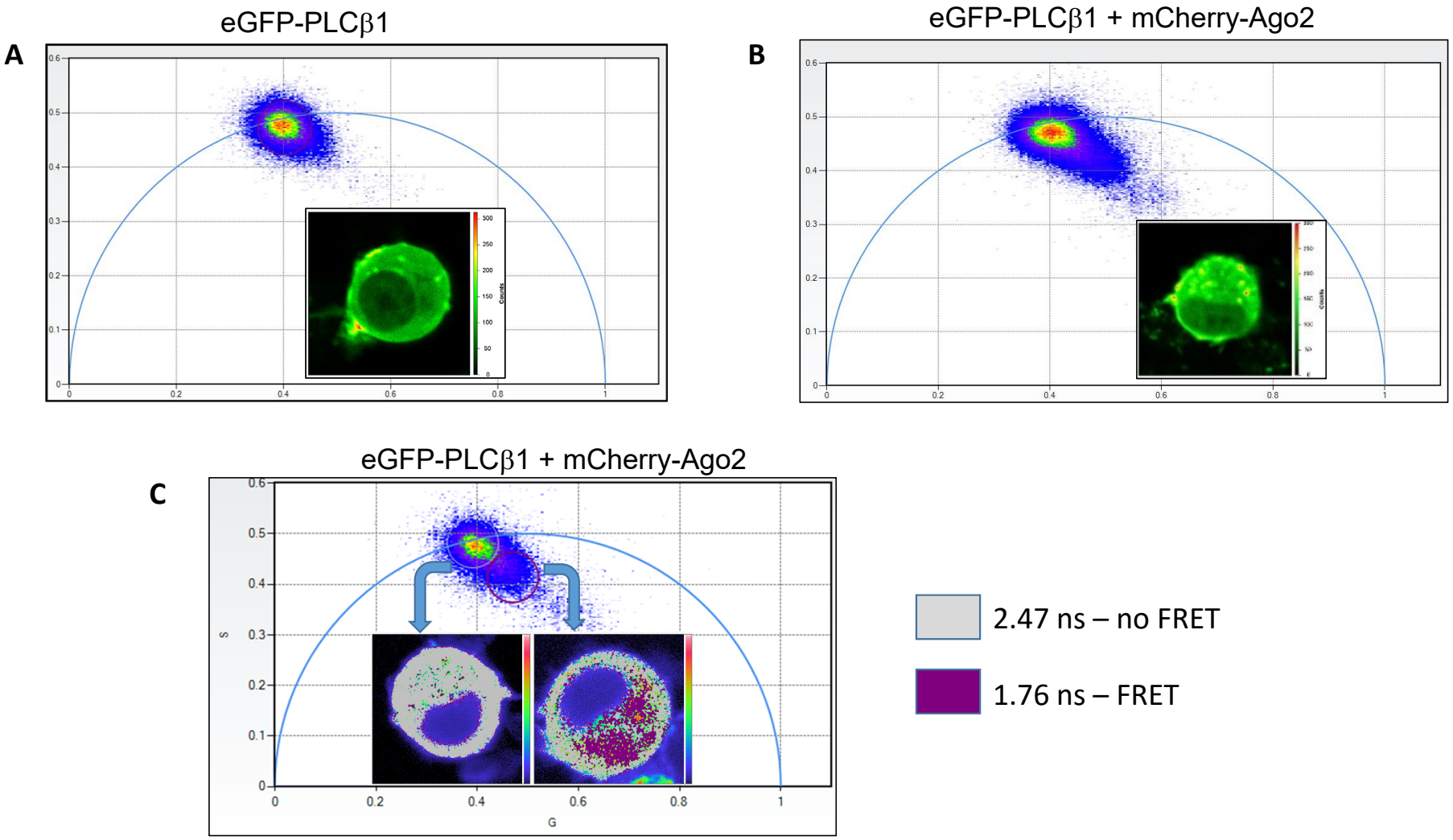

Fig. 4

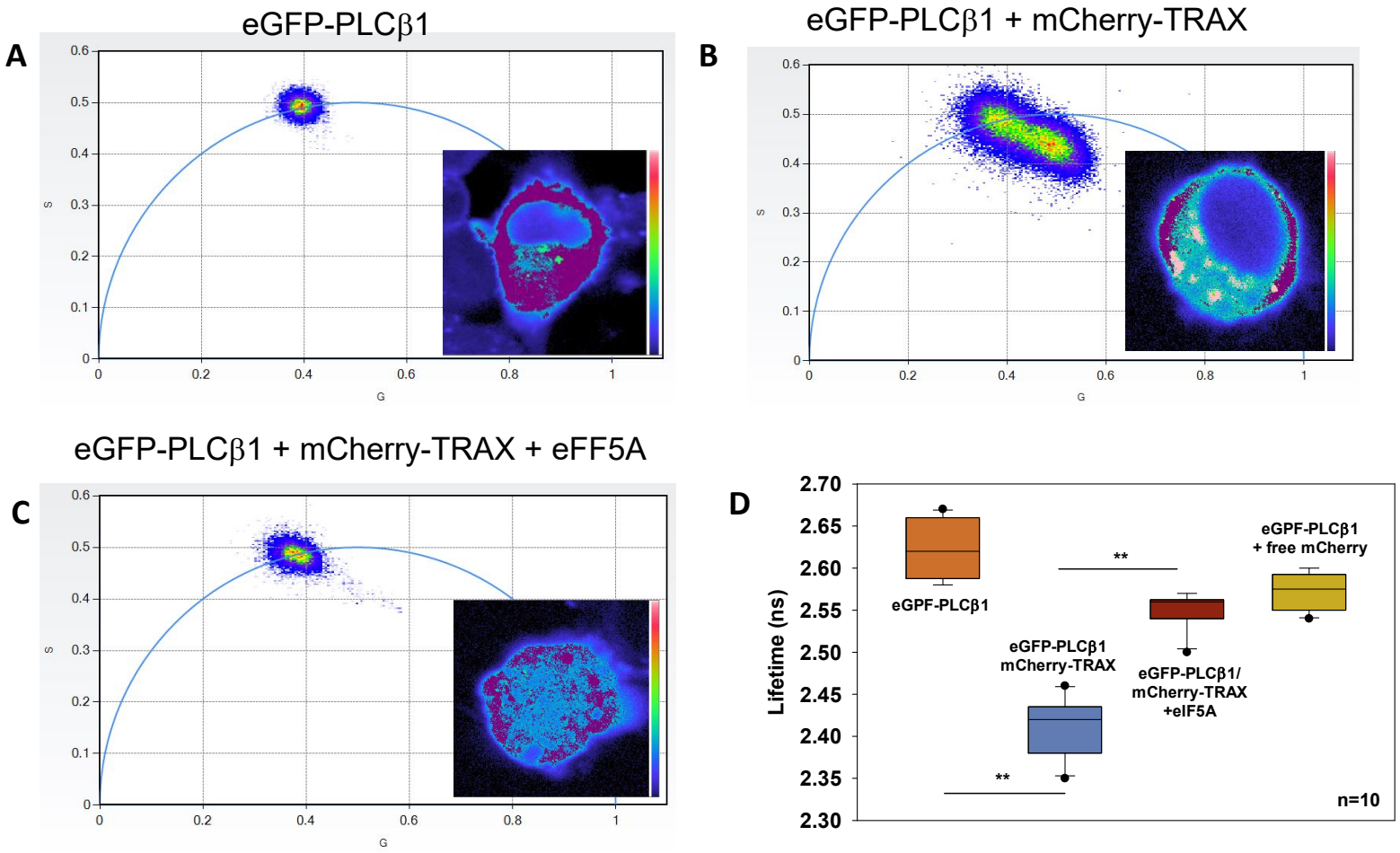

Fig. 5 put in statement or data showing basal

A

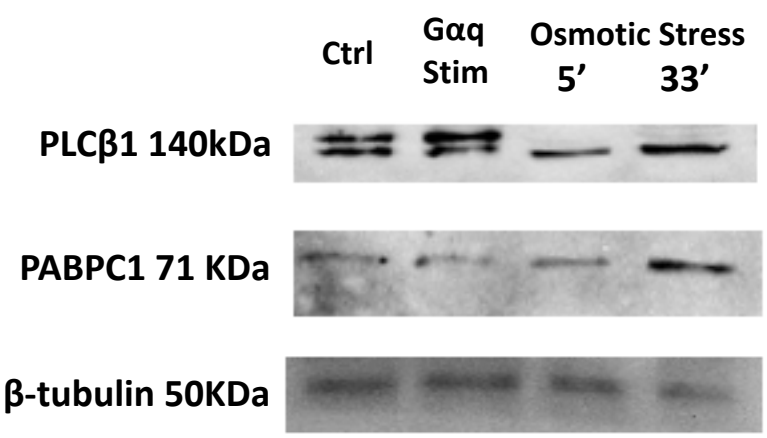

B

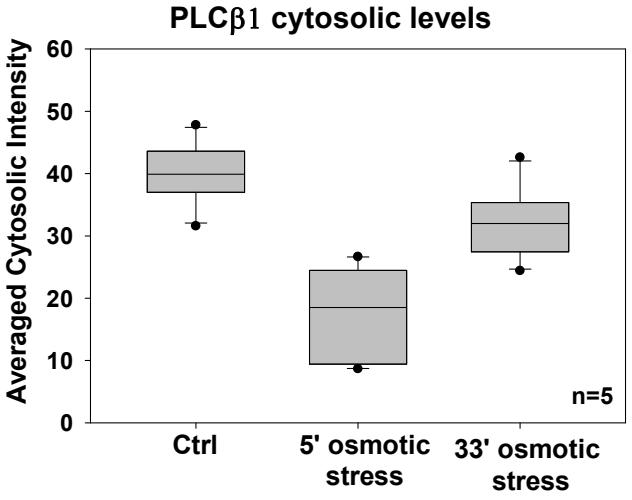

C

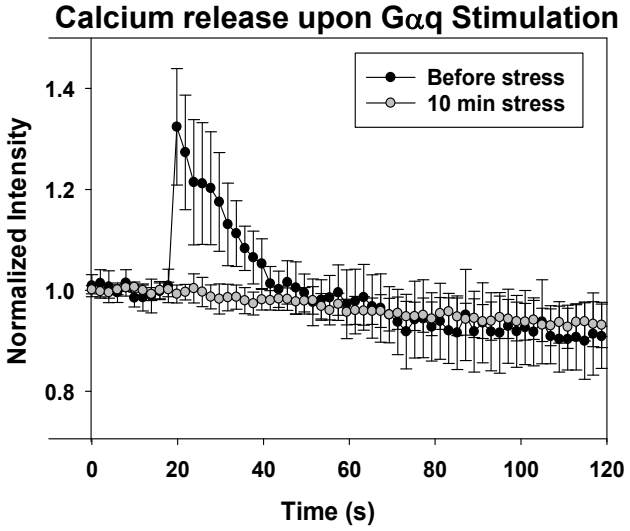

Fig.6

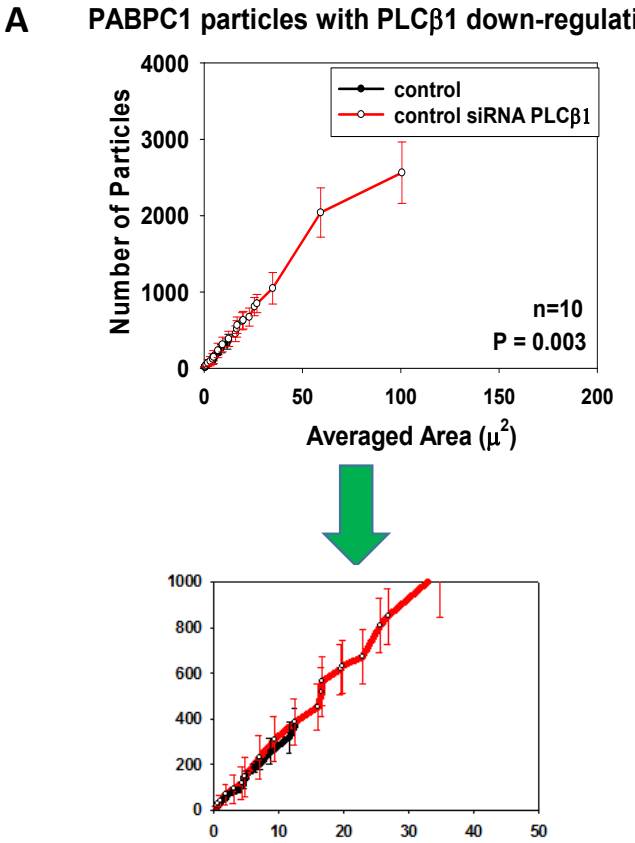

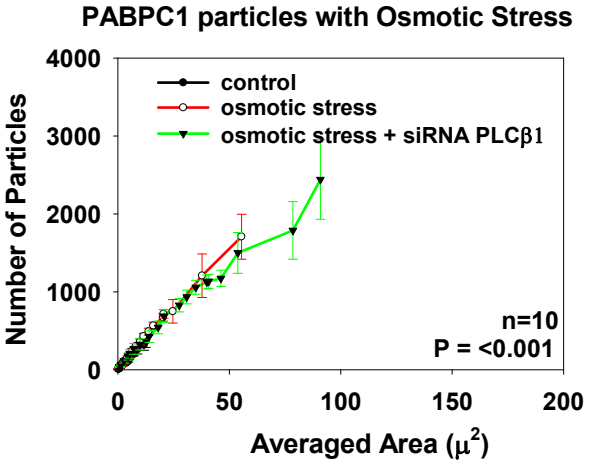

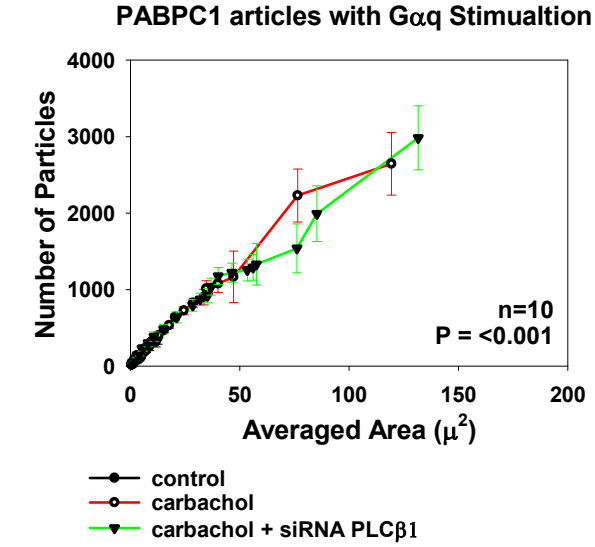

Fig. 7

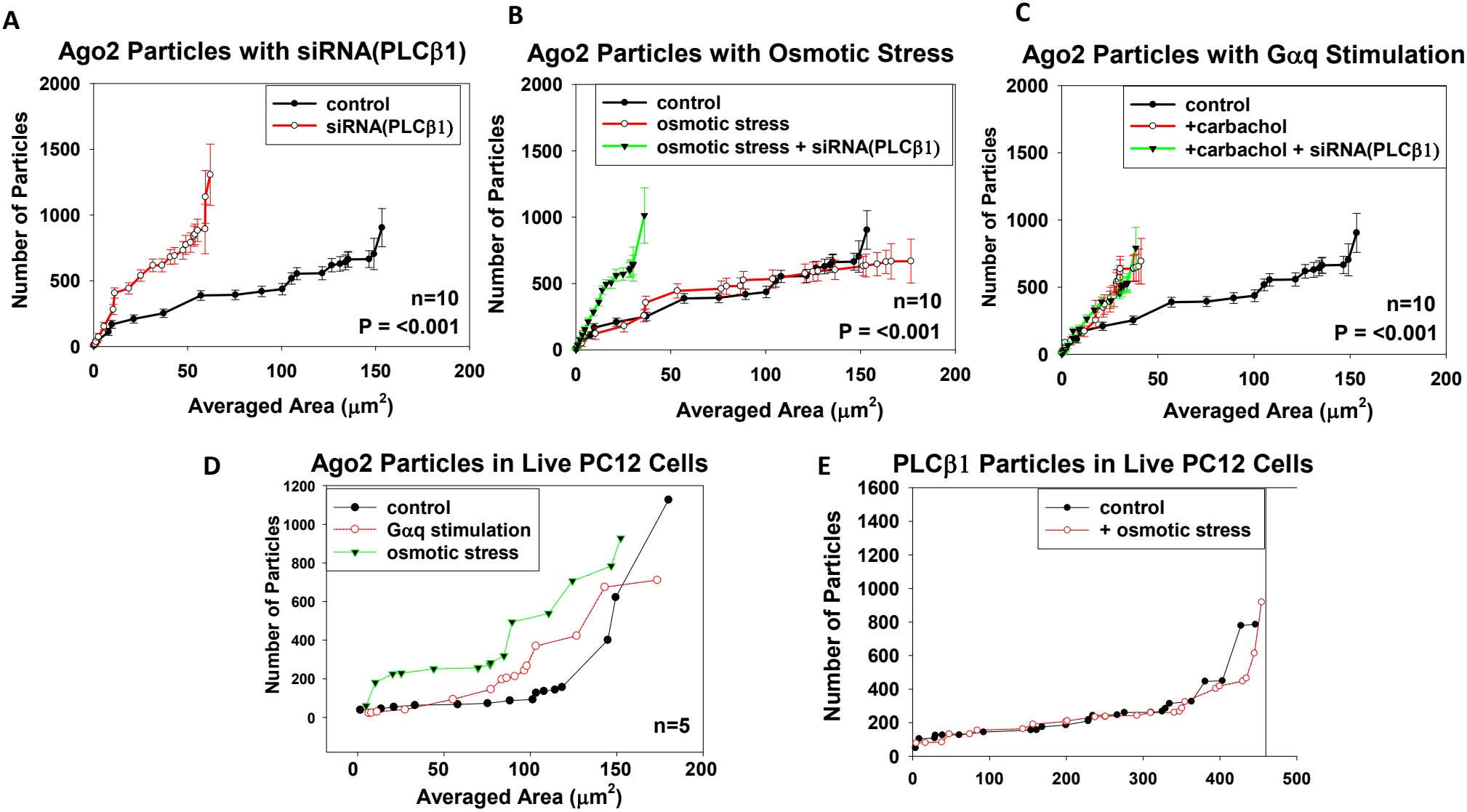

Fig 8

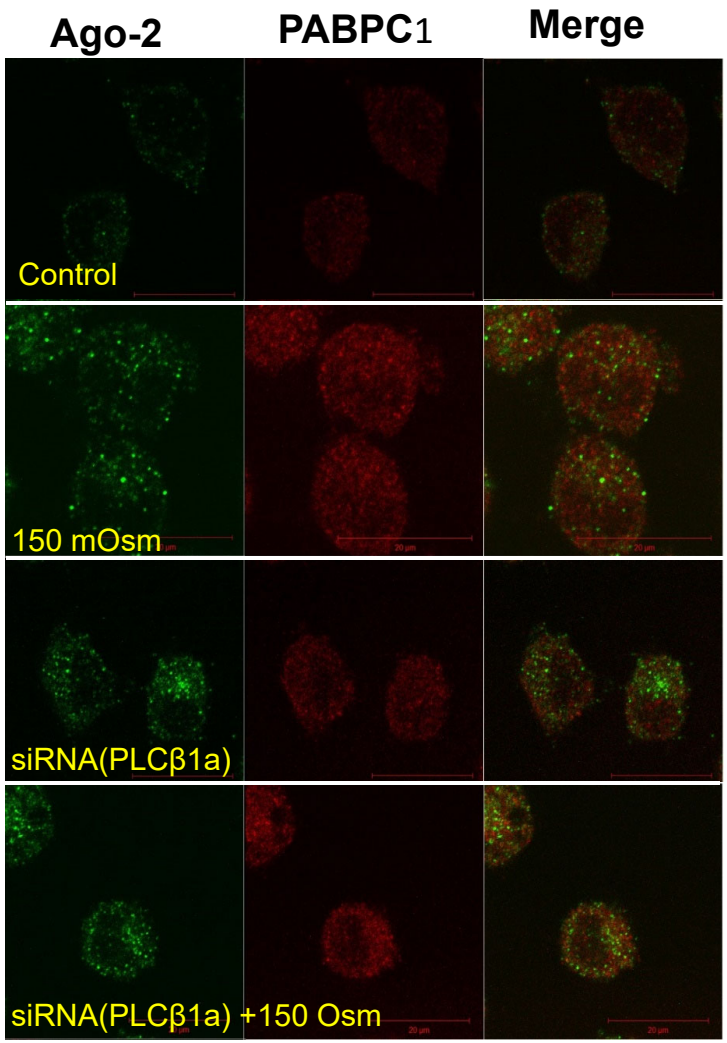

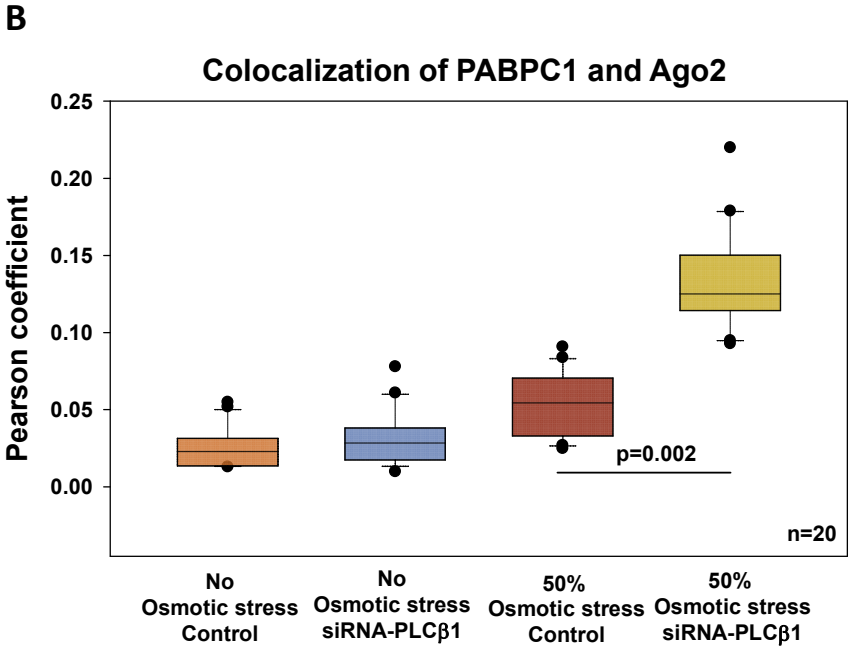

Fig. 9

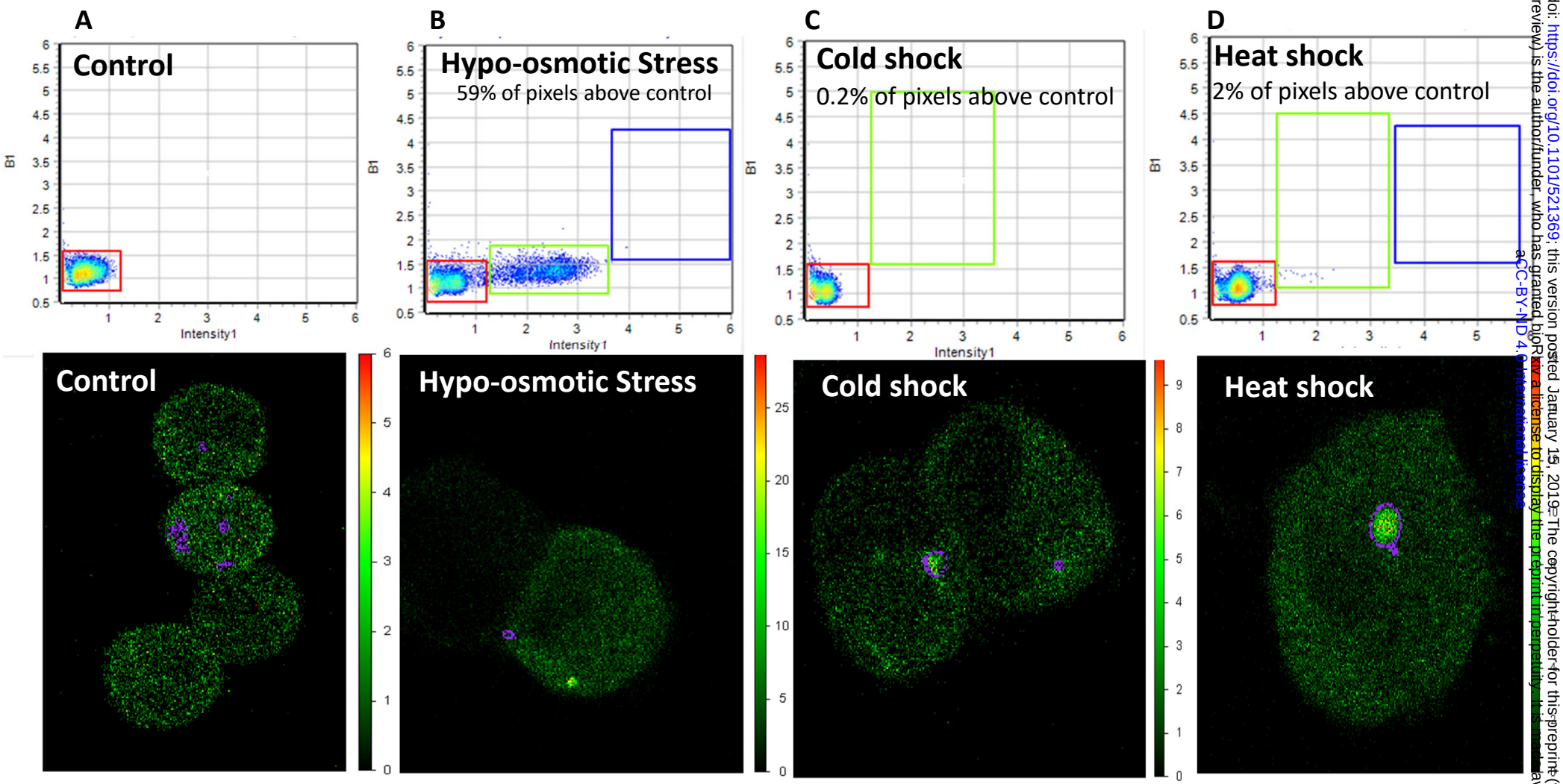

Fig. 10

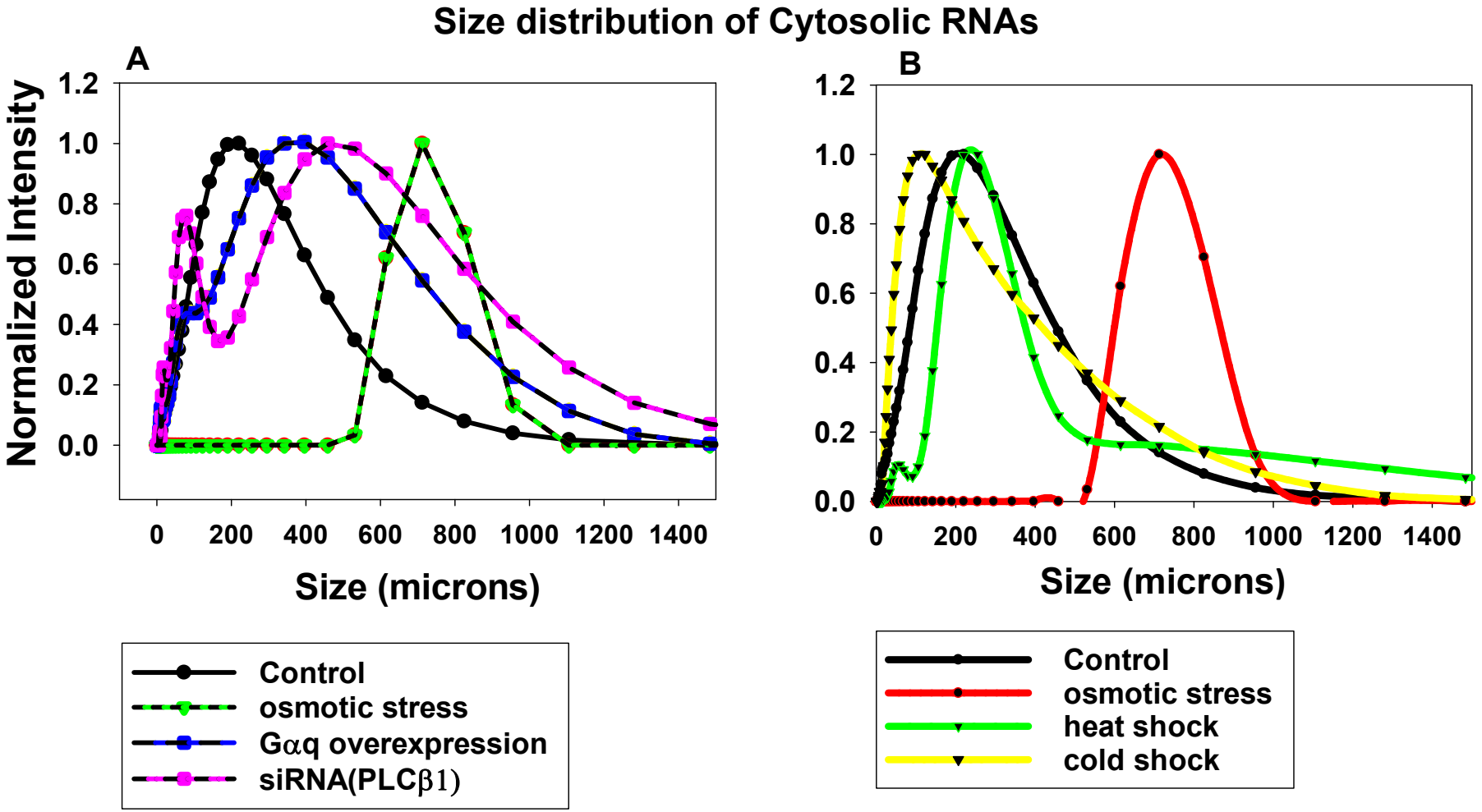

Fig. 11

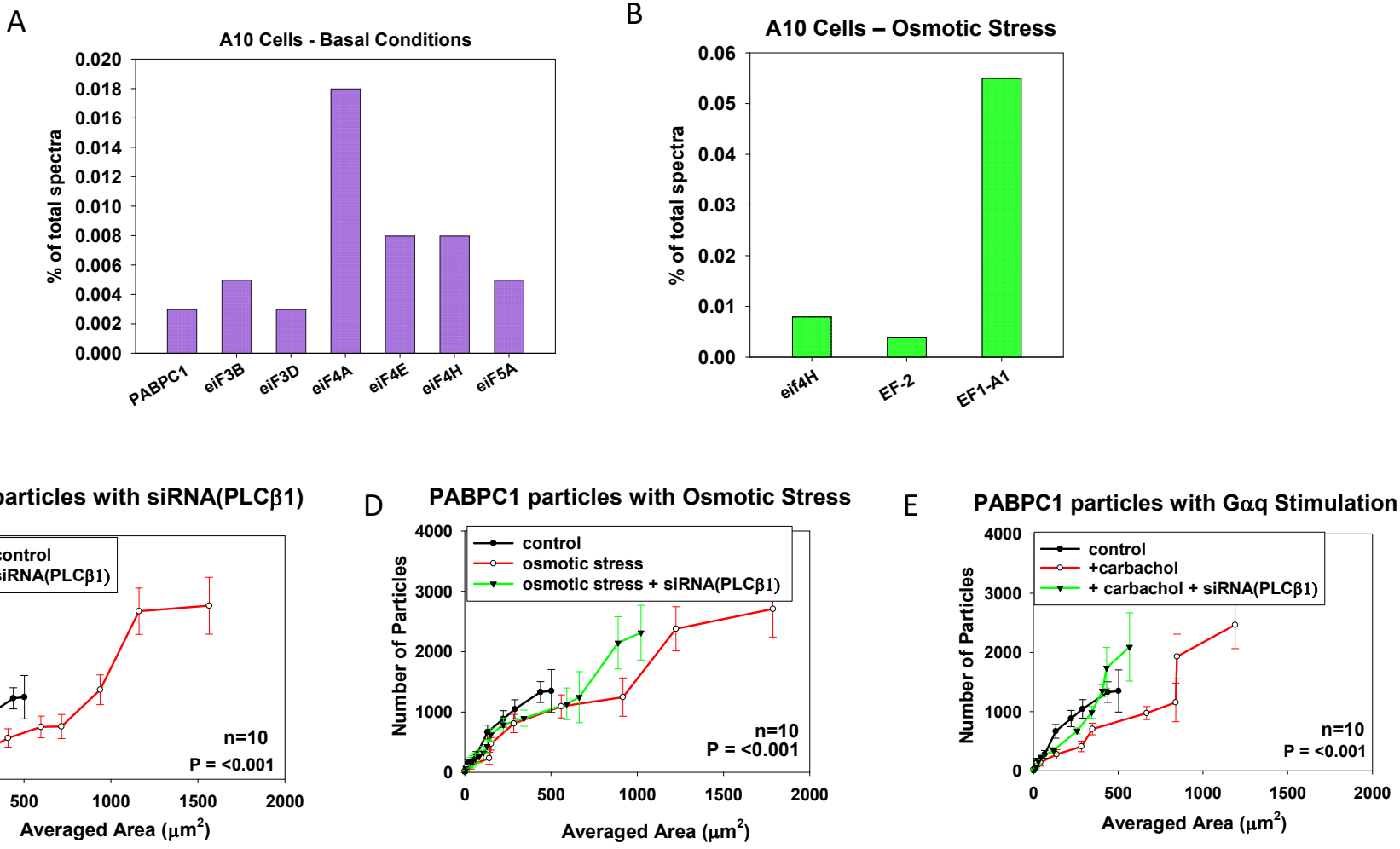

Fig. 12